Chemical Engineering Journal 419 (2021) 129517

Contents lists available at ScienceDirect

Chemical Engineering Journal

journal homepage: www.elsevier.com/locate/cej

Amine blending optimization for maximizing CO_2 absorption capacity in a diisopropanolamine – methyldiethanolamine – H_2O system using the electrolyte UNIQUAC model

Bong Keun Choi [a], Seung-Mo Kim [a], Kyung-Min Kim [b], Ung Lee [c], Jeong Ho Choi [d], Jong-Seop Lee [d], Il Hyun Baek [d], Sung Chang Nam [d,*], Jong-Ho Moon [a,*]

[a] Department of Chemical Engineering, Chungbuk National University, Cheongju, Chungbuk 28644, South Korea
[b] Department of Biochemical Engineering, Gangneung-Wonju National University, Gangneung, Ganwon 25457, South Korea
[c] Korea Institute of Science and Technology, Hwarang-ro 14-gil 5, Seongbuk-gu, Seoul 02792, South Korea
[d] Korea Institute of Energy Research, 102 Gajeong-ro, Yuseong-gu, Daejeon 34129, South Korea

ARTICLE INFO

Keywords:
CO_2 solubility
Diisopropanolamine (DIPA)
Methyldiethanolamine (MDEA)
Blended amine
Electrolyte universal quasi-chemical (electrolyte UNIQUAC) model
Cyclic capacity

ABSTRACT

Experimental data on CO_2 solubility in diisopropanolamine (DIPA) and methyldiethanolamine (MDEA) blended aqueous solutions were measured at different amine blending ratios and working temperatures. The successive (iterative) substitution method was implemented to calculate the molar fractions of all chemical species, including molecules and electrolytes, from equilibrium along with four material balances and one electroneutrality equation. The electrolyte universal quasi-chemical (electrolyte UNIQUAC) model was used to consider the nonideality in the liquid phase. The partial pressures of CO_2 in the gas phase and molar fractions of all components in the liquid phase were recalculated using thermodynamic models. In addition, the effect of the blending ratio of DIPA, MDEA, and H_2O was investigated and expressed using the newly applied triangular diagrams of pH, heat of absorption, and cyclic capacity of CO_2 according to the absorption and stripping conditions.

1. Introduction

Carbon capture and storage (CCS) is an effective strategy for directly reducing anthropogenic CO_2 emissions. Various methods, including absorption, adsorption, and membrane technologies, have been suggested for the separation of CO_2 from off-gas. Chemical absorption is considered to be the most developed technique and has already been successfully applied in the chemical industry, for example, in the gas sweetening process. One approach to enhance the feasibility of the absorption process is to use an effective solvent with characteristics such as a high loading capacity, high stability, low regeneration energy, and fast reaction rates [1].

Many studies have reported on the potential of various single and blended amines [2–8], recently. At present, new amine CO_2 absorbent have been studied. Blending two or more amines, such as the main amine and promotor, with water is widely applied to CO_2 absorption solvents. It can match solvents with different physical and chemical characteristics, improve the absorption equilibrium and kinetics, control the heat of absorption and pH, and prevent corrosion and solvent degradation [2,9,10]. Commercial amines can be categorized into four types: primary amines such as monoethanolamine (MEA); secondary amines such as diethanolamine (DEA) and diisopropanolamine (DIPA); tertiary amines such as triethanolamine (TEA), triethylamine (TREA), and methyldiethanolamine (MDEA); and steric hindrance amines such as 2-amino-2-methyl propanol (AMP). DIPA, a secondary amine, has been reported to exhibit a high selectivity toward CO_2; it is also less corrosive. In addition, it can remove H_2S and COS without excessive degradation, and require less heat in the regeneration of the solution [11–13]. MDEA, which is a tertiary amine, shows excellent chemical and thermal stability and low-corrosive behavior [14]. In blended DIPA and

Abbreviations: AMP, 2-amino-2-methyl-propanol; CCS, carbon capture and storage; DEA, diethanolamine; DIPA, diisopropanolamine; MDEA, methyldiethanolamine; MEA, monoethanolamine; NRTL, nonrandom two liquid; UNIQUAC, universal quasi chemical; SMAPE, symmetric mean absolute percentage error; TEA, triethylamine; VLE, vapor–liquid equilibrium.

* Corresponding authors.
E-mail addresses: scnam@kier.re.kr (S.C. Nam), moonjongho@chungbuk.ac.kr (J.-H. Moon).

https://doi.org/10.1016/j.cej.2021.129517
Received 3 January 2021; Received in revised form 18 March 2021; Accepted 20 March 2021
Available online 29 March 2021

MDEA aqueous amine system, very little experimental data have been reported. Jenab et al. [15] and Vahidi et al. [12] measured CO_2 solubility in a blended DIPA and MDEA aqueous solution at 313.15–358.2 K. In the present study, the CO_2 absorption characteristics in aqueous DIPA and MDEA blended solutions were examined at wide range of temperature, 323.15–383.15 K (absorption condition to desorption condition), through experiments and by using thermodynamic models.

Vapor-liquid-equilibrium (VLE) data for CO_2 absorption in aqueous alkanolamine solutions is essential for the design of amine-based acid gas removal units. Thermodynamic models can be established by fitting the model equation to the experimental data. Thermodynamic modeling can be classified into three approaches. The first involves obtaining new chemical equilibrium constants related to amines, such as carbamate formation or amine protonation. Kent and Eisenberg proposed a very useful and simple model, which neglected the activity coefficients. The Aroua group [16,17] predicted CO_2 solubility in various amine solutions using the Kent and Eisenberg model. The second approach uses excess Gibbs energy models. Deshmukh and Mather proposed activity coefficient models using the Guggenheim equation [18–22]. The Aroua group [23], Mather group [18,20,21,24], Pahlavanzadeh group [25], and Mofarahi group [9,26,27] have adapted the above models to predict CO_2 solubility in various amine–water systems. The last approach, also called the electrolyte model, uses excess Gibbs energy. Chen et al. proposed an electrolyte nonrandom two-liquid (electrolyte NRTL) model. The electrolyte NRTL model consists of three terms: i) the Pitzer–Debye–Hückel term, a description of long-range electrostatic interactions, ii) NRTL model, and iii) an expression for the short-range van der Waals interactions [28,29]. The Chen group [28,30–32], Rochelle group [33–35], and Svendsen group [36–38], adapted the electrolyte NRTL model to various CO_2–amine–H_2O systems. Previously, our group compared the Kent and Eisenberg model and excess Gibbs energy models (electrolyte NRTL model and Deshmukh–Mather model) with the MDEA–CO_2–H_2S–H_2O system [39].

Recently, several research papers have been published that calculate the activity coefficient by applying an electrolyte system to the UNIQUAC model. Three different types of electrolyte universal quasichemical (electrolyte UNIQUAC) models have been applied. The Svendsen group [40–42] and the Yesavage group [43] applied the extended UNIQUAC model, the Haghtalab group [44,45] applied the electrolyte UNIQUAC-NRF model, and the Al-Rashed group [46] applied the electrolyte UNIQUAC model. In addition, to predict the CO_2 solubility in a blended amine aqueous solution, the electrolyte UNIQUAC model was used in the reported literature [43,46]. The electrolyte UNIQUAC model proposed by Al-Rashed [43,46] is a combination of the Debye–Hückel term, which accounts for long-range ion–ion interactions, and the UNIQUAC expression proposed by Abrams and Praunitz [47] to account for all types of short-range interactions. This model uses the molecule, ion size, and shape parameter to consider the short-range interactions. In addition, it assumes that short-range interactions occur between the ion–ion pairs. This assumption considerably simplifies the expression for the activity coefficient.

To analyze CO_2 absorption behaviors in the DIPA–MDEA–H_2O system, the mole fraction of all species (four molecules and seven electrolytes) in the liquid phase must be accurately calculated to a level of $\leq 10^{-14}$. In addition, to obtain the above mole fraction of all species, it is necessary to solve 11 equations, which include six equilibriums, four material balances, and one electroneutrality, simultaneously with low relative tolerances ($<10^{-7}$). In CO_2–primary or secondary amine–H_2O systems, CO_2 reacts with amines and H_2O to form both carbamate ($DIPACOO^-$ in this study) and bicarbonate (HCO_3^-) ions. On the other hand, in CO_2–tertiary amine–H_2O systems, carbamate ions are not formed when CO_2 reacts with the amines. Therefore, the behavior of carbamate and bicarbonate ions is useful in the mixture of secondary and tertiary amine aqueous solutions, such as DIPA and MDEA in the present work.

In this study, the effects of the blending ratio in DIPA–MDEA–H_2O and the temperature on CO_2 solubility were investigated. The CO_2 solubility in an aqueous solution of blended DIPA and MDEA was newly measured over a wide range of temperatures (absorption condition of 323.15 K and desorption condition of 383.15 K). The successive substitution method [39,48–50] was implemented to calculate the mole fractions of all species in the liquid phase, such as molecules and electrolytes. The CO_2 partial pressure in the gas (vapor) phase was estimated using the gamma (activity, γ)–phi (fugacity, Φ) approach. The electrolyte UNIQUAC model, an activity coefficient model, was used to calculate the nonideality of the liquid phase. Other important characteristics related to the CO_2 absorption processes according to the DIPA–MDEA–H_2O blending ratios were evaluated using in-house MATLAB codes, such as the molar fraction of the liquid phase, the behavior of bicarbonate and carbamate ions, pH, heat of absorption, and cyclic capacities of CO_2 ($\Delta\alpha_{CO_2}$).

2. Experimental

2.1. Materials

DIPA (≥98%, JUNSEI), MDEA (≥99%, Sigma-Aldrich), and distilled water were blended to prepare the absorption solutions. The concentration of the aqueous blended amine solution was 30 wt% (70 wt% H_2O). The mass ratios of DIPA and MDEA were 3:7, 5:5, and 7:3, respectively. That is, the mass fractions of DIPA and MDEA were 0.09:0.21, 0.15:0.15, and 0.21:0.9, and the mass fraction of distilled water was 0.70 (70 wt%). Pure CO_2 (≥99.99%) and pure N_2 (≥99.999%) were used in the present work.

2.2. Experimental method

The solubility of CO_2 in the DIPA–MDEA blended aqueous solutions was measured between 323.15 K (absorption condition) and 383.15 K (desorption condition). In the present work, an experimental procedure is used that based on static method and is same as the work of Moon et al. [39] The first step, cleaning step, distilled water and pure nitrogen were used to wash the reactor three times. The gases in the reactors were analyzed by on-line gas chromatography (Agilent Co., 7890 series) to confirm if any gases other than nitrogen remained in the reactor. Then, the reactor was washed once again with pure nitrogen and an aqueous amine solution before use in the experiment. After washing, the reactor was heated to the experimental temperature. In the CO_2-absorption step, ~150 g of the prepared amine solution was injected into the reactor using a high-pressure syringe pump. The pressure was measured when the temperatures of the gas and the injected amine solution became constant. The vapor pressure was obtained using the pressure change of the reactor, the amount of the injected solution, and the volume of the reactor. After the solution-injection step, CO_2 was introduced into the reactor. To increase the contact possibility between the amine solution and the CO_2 molecules, a magnetically driven impeller-type stirrer, installed in the reactor, was used. Initially, the pressure of the reactor decreased because of CO_2 absorption in the solution. If the pressure became constant for 1 h, it was regarded that the absorption equilibrium had been reached, and the pressure was measured; Typically, the first step takes about 10 to 15 h in total to reach equilibrium, and the next steps take about 3 to 5 h. Then, the feed CO_2 in the gas reservoir was reintroduced into the reactor. After the absorption experiment, the experimental procedure was returned to the cleaning step.

The experimental CO_2 solubility can be shown with the CO_2-loading ratio and the molar ratio of gaseous CO_2 per total amine in the liquid phase. The equilibrium CO_2-loading ratio (α_{CO_2}, mol CO_2/total mol amine) was calculated from the partial pressure and the quantity of the absorbed CO_2 at each equilibrium step using Eq. (1), as follows:

$$\alpha_{CO_2} = \frac{n_{CO_2,liq}}{\sum n_{amine,liq}} \quad (1)$$

where $n_{CO_2,liq}$ is the number of moles of CO_2 in the liquid phase, and $\sum n_{amine,liq}$ is the total number of moles of the blended amine (DIPA and MDEA in this study) in the liquid phase. Then, the Redlich–Kwong equation was applied to calculate the amount of absorbed CO_2. The uncertainty of the experimental data on CO_2 partial pressure was estimated using the equation presented by NIST [51] and Kim et al.[52]. Detailed information on the uncertainty and the experimental devices are provided in the Supporting Information.

3. Model and optimization

3.1. Chemical and phase equilibrium in the blended amine aqueous system

In a blended amine aqueous solution, CO_2 reacts with H_2O and amines. Zhong and Chen [53], Haghtalab et al. [54], and Vahidi et al. [12] used the equilibrium expression in which bicarbonate reacts with amine to form carbamate. Also, Barth et al. [55], Blauwhoff et al. [56], Littel et al. [57], and Vaidya's group [58,59] reported the reaction mechanism in which CO2 reacts DIPA, directly. In the present work, carbamate ion (in this study, DIPACOO–) is assumed to be formed by the reaction of bicarbonate with amine [54] (in this study, DIPA). For the CO_2–DIPA–MDEA–H_2O system, the reactions take place in the liquid phase as follows:

Alkanolamine (DIPA): DIPAH+ + H2O ↔ DIPA + H3O+ (2)

Alkanolamine (MDEA): MDEAH+ + H2O ↔ MDEA + H3O+ (3)

Carbon dioxide: CO2 + 2H2O ↔ H3O+ + HCO3– (4)

Bicarbonate: HCO3– + H2O ↔ H3O+ + CO32– (5)

Water: 2H2O ↔ H3O+ + OH– (6)

Carbamate: DIPACOO– + 2H2O ↔ DIPA + HCO3– (7)

The equilibrium constants (K_j (-)) for the above reactions can be described as follows:

$$K_1 = \frac{x_{DIPA}x_{H_3O^+}}{x_{DIPAH^+}x_{H_2O}} \cdot \frac{\gamma_{DIPA}\gamma_{H_3O^+}}{\gamma_{DIPAH^+}\gamma_{H_2O}} \quad (8)$$

$$K_2 = \frac{x_{MDEA}x_{H_3O^+}}{x_{MDEAH^+}x_{H_2O}} \cdot \frac{\gamma_{MDEA}\gamma_{H_3O^+}}{\gamma_{MDEAH^+}\gamma_{H_2O}} \quad (9)$$

$$K_3 = \frac{x_{H_3O^+}x_{HCO_3^-}}{x_{CO_2}x_{H_2O}^2} \cdot \frac{\gamma_{H_3O^+}\gamma_{HCO_3^-}}{\gamma_{CO_2}\gamma_{H_2O}^2} \quad (10)$$

$$K_4 = \frac{x_{H_3O^+}x_{CO_3^{2-}}}{x_{HCO_3^-}x_{H_2O}} \cdot \frac{\gamma_{H_3O^+}\gamma_{CO_3^{2-}}}{\gamma_{HCO_3^-}\gamma_{H_2O}} \quad (11)$$

$$K_5 = \frac{x_{H_3O^+}x_{OH^-}}{x_{H_2O}^2} \cdot \frac{\gamma_{H_3O^+}\gamma_{OH^-}}{\gamma_{H_2O}^2} \quad (12)$$

$$K_6 = \frac{x_{DIPA}x_{HCO_3^-}}{x_{DIPACOO^-}x_{H_2O}} \cdot \frac{\gamma_{DIPA}\gamma_{HCO_3^-}}{\gamma_{DIPACOO^-}\gamma_{H_2O}} \quad (13)$$

where x_i (-) is the molar fraction and γ_i (-) is the activity coefficient of species i. Eqs. (8)–(13) should simultaneously satisfy the material balance and electrical neutrality (the charge balance), as shown below:

$$x'_{MEA} = x_{MEA} + x_{MEAH^+} + x_{MEACOO^-} \quad (14)$$

$$x'_{AMP} = x_{AMP} + x_{AMPH^+} \quad (15)$$

$$x'_{CO_2} = x_{CO_2} + x_{HCO_3^-} + x_{CO_3^{2-}} + x_{MEACOO^-} \quad (16)$$

$$x'_{H_2O} = x_{H_2O} + x_{H_3O^+} + x_{OH^-} + x_{HCO_3^-} + x_{CO_3^{2-}} \quad (17)$$

$$x_{MEAH^+} + x_{AMPH^+} + x_{H_3O^+} = x_{HCO_3^-} + 2x_{CO_3^{2-}} + x_{OH^-} + x_{MEACOO^-} \quad (18)$$

In the present work, 11 variables (four molecules and seven electrolytes) were solved simultaneously using 11 equations (six equilibrium expressions, four material balances, and one electroneutrality) by employing the successive substitution method. To solve the multiphase equilibrium and chemical equilibrium, successive substitution method has been reported in the literature [49,50]. In the present study, successive substitution method was modified for the DIPA and MDEA blended amine aqueous systems [39]. The relative tolerance was set to under 10^{-7} for all the 11 variables.

The partial pressure of CO_2 and the liquid-phase concentration of CO_2 were calculated using the phase equilibrium formula as follows: [33,34,54]

$$\phi_{co_2} y_{co_2} P = H_{co_2}\gamma_{co_2} x_{co_2} \exp\left(\frac{\bar{v}^{\infty}_{co_2}(P - P^0)}{RT}\right) \quad (19)$$

For the solvent species, s (DIPA, MDEA, and H_2O in this study), the phase equilibrium formula can be written as follows:

$$\phi_s y_s P = x_s\gamma_s P^0_s \phi^0_s \exp\left(\frac{v_s(P - P^0_s)}{RT}\right) \quad (20)$$

where ϕ_i (-) is the fugacity coefficient, y_i (-) is the molar fraction of the vapor phase, P (Pa) is the system total pressure, H_{co_2} (Pa) is Henry's constant, $\bar{v}^{\infty}_{co_2}$ (cm^3/mol) is the infinite dilution partial molar volume, and v_s is the molar volume of the pure solvent at the system temperature and saturation pressure. The equation suggested by Prausnitz et al. [60] was used to determine ϕ_i. The infinite dilution partial molar volume ($\bar{v}^{\infty}_{co_2}$) was calculated using the Brelvi–O'Connell model [61]. P^0 is the saturated vapor pressure obtained by the Antoine equation [60]. The Antoine equation coefficients for DIPA and MDEA are listed in Table 1. Henry's constant in the mixed solvents was calculated using the volume weighted mixing rule as follows [32,54,62].

$$\ln\left(\frac{H_{co_2}}{\gamma^{\infty}_{co_2}}\right) = \sum_A w_A \ln\left(\frac{H_{co_2,A}}{\gamma^{\infty}_{co_2,A}}\right) \quad (21)$$

where w_A is the weighting factor (-), H_{co_2} and $\gamma^{\infty}_{co_2}$ are Henry's constant and the infinite dilution activity coefficient of CO_2 in the mixed solvent, respectively, and $H_{co_2,A}$ and $\gamma^{\infty}_{co_2,A}$ are Henry's constant and the infinite dilution activity coefficient of CO_2 in pure solvent A, respectively. In the vapor and liquid-phase equilibria of the blended amine aqueous amine solution, two types of species exist, such as molecular and ionic species. In this study, it was assumed that the presence of ionic species in the vapor phase can be ignored.

The equilibrium constant (K_j) for the j^{th} reaction and Henry's constant ($H_{co_2,s}$) for CO_2 in solvent, s, can be described as temperature-dependency expressions:

Equilibrium constant:

Table 1
Antoine equation coefficients obtained for vapor pressure (P^o_s).

s	A	B	C	Reference
DIPA[a]	11.18	–2009.3	–224.15	Klepacova et al. [75]
MDEA[b]	10.182	–3578.6	264.24	Kim et al. [74]
H_2O[c]	5.11564	–1687.537	230.17	Reid et al. [76]

[a] $ln(P^o_s/kPa) = A + \frac{B}{C + (T/K)}$.

[b] $log_{10}(P^o_s/mm\ Hg) = A + \frac{B}{C + (T/^{\circ}C)}$.

[c] $log_{10}(P^o_s/bar) = A + \frac{B}{C + (T/K)}$.

$$\ln(K_j) = A_1 + A_2/T + A_3 \ln T + A_4 T \quad (22)$$

Henry's constant:

$$\ln(H_{co_2,s}) = B_1 + B_2/T + B_3 \ln T + B_4 T \quad (23)$$

The temperature-dependent coefficients for K_j (A_1–A_4) and $H_{co_2,s}$ (B_1–B_4) are listed in Tables 2 and 3, respectively.

3.2. Activity coefficient model: Electrolyte UNIQUAC

The electrolyte UNIQUAC model proposed by Al-Rashed and Ali [46] is used to consider the nonidealities of liquid phases in an aqueous electrolyte system. This model can estimate the activity coefficients for the molecular and ionic species using binary and ion-pair parameters. Electrolyte UNIQUAC is an excess Gibbs energy model that follows two assumptions for ion-pair formation [30,31]: (i) Like-ion repulsion, in which large repulsive forces between ions of the same charge, ion pairs, or ion triplets cannot form among ions of the same charge, and (ii) local electroneutrality, which requires that the local net ionic charge be zero in the solution. This implies that cations and anions may form ion pairs or ion triplets in such a way that their net charge is zero. The electrolyte UNIQUAC model can be considered as the sum of three terms as follows [46]:

$$\frac{g^{ex*}}{RT} = \frac{g^{ex*,dh}}{RT} + \frac{g^{ex*,C}}{RT} + \frac{g^{ex*,R}}{RT} \quad (24)$$

where g^{ex*} is the excess Gibbs energy of the mixed solvent electrolyte system, $g^{ex*,dh}$ is the excess Gibbs energy calculated using the Debye–Hückel formula, and $g^{ex*,C}$ and $g^{ex*,R}$ are the excess Gibbs energy calculated using the electrolyte UNIQUAC model, combinatorial term, and residual term, respectively. The activity coefficients for species i were obtained by differentiating the excess Gibbs function (Eq. (24)), which can be expressed as follows:

$$\ln\gamma_i = \left[\frac{\partial(n_t g^{ex*}/RT)}{\partial n_i}\right]_{T,P,n_{j\neq i}} \quad (25)$$

$$\ln\gamma_i = \ln\gamma_i^{dh} + (\ln\gamma_i^{C} + \ln\gamma_i^{R}) \quad (26)$$

The first term of Eq. (26), $\ln\gamma_i^{dh}$, represents the contribution to the long-range electrostatic forces. The Debye–Hückel formula was proposed by Fowler and Guggenheim [63] and modified by Macedo and coworkers [64]. The Debye–Hückel activity coefficients for solvent and molecular component k and ion component i are given below:

$$\ln\gamma_k^{dh} = \frac{2AM_k\rho_s}{b^3\rho_k}\left\{1 + bI_m^{1/2} - 1/\left(1 + bI_m^{1/2}\right) - 2\ln\left(1 + bI_m^{1/2}\right)\right\} \quad (27)$$

$$\ln\gamma_i^{*,dh} = -\frac{Az_i^2 I_m^{1/2}}{1 + bI_m^{1/2}} \quad (28)$$

$$A = \frac{e^3}{k^{3/2}}(2\pi N_0)^{1/2} \times \frac{\rho_s^{1/2}}{(\varepsilon T)^{3/2}} \quad (29)$$

Table 2
Temperature-dependent coefficients (A_1–A_4) for the reaction equilibrium constants, K_j (mole fraction basis).

K_j [a]	A_1	A_2	A_3	A_4	Reference
K_1	–12.4953	–3556.50	0.0	0.0	Barth et al. [55]
K_2	–9.4165	–4234.98	0.0	0.0	Schwabe et al. [77]
K_3	231.465	–12092.1	–36.7816	0	Edwards et al. [78]
K_4	216.049	–12431.7	–35.4819	0	Edwards et al. [78]
K_5	132.899	–13445.9	–22.4773	0	Edwards et al. [78]
K_6	5.20402	–3173.9	0.0	0.0	Blauwhoff et al. [56]

[a] $\ln(K_j) = A_1 + A_2/T + A_3 \ln T + A_4 T$; the unit for temperature T is K.

Table 3
Temperature-dependent coefficients (B_1–B_4) obtained for the Henry's constants ($H_{CO_2,s}$).

$H_{co_2,s}$	B_1	B_2	B_3	B_4	reference
[a]H_{CO_2,H_2O}	94.4914	–6789.04	11.4519	–0.0010454	Edwards et al. [78]
[b]$H_{CO_2,DIPA}$	19.3104	–1427.9	0	0	Zong and Chen [53]
[b]$H_{CO_2,MDEA}$	19.8933	–1072.7	0	0	Zhang and Chen [62]

[a] $\ln(H_{co_2,H_2O}) = B_1 + B_2/(T/K) + B_3\ln(T/K) + B_4(T/K)$; the unit for H_{co_2,H_2O} is kg-atm/mol.
[b] $\ln(H_{co_2,s}) = B_1 + B_2/(T/K) + B_3\ln(T/K) + B_4(T/K)$; the unit for $H_{co_2,s}$ is Pa.

$$b = \frac{ae}{k}(8\pi N_0)^{1/2} \times \frac{\rho_s^{1/2}}{(\varepsilon T)^{1/2}} \quad (30)$$

$$I_m = \frac{1}{2}\sum_{i=1}^{N_{ion}} m_i z_i^2 \quad (31)$$

where γ_k^{dh} is the Debye–Hückel activity coefficient for the solvent and molecular component k (-), $\gamma_i^{*,dh}$ is the Debye–Hückel activity coefficient for ion component i (-), A and b are the Debye–Hückel parameters ($kg^{1/2}/mol^{1/2}$), M_k is the molecular weight of component k (kg/mol), ρ_s and ρ_k are the densities of the mixed solvent mixture and pure solvent k, respectively, I_m is the ionic strength on the molarity scale (mol/kg), m_i is the molarity of ion i (mol/kg), z_i is the charge number of ion i (-), e is the electron charge (C), k is the Boltzmann constant (J/K), N_0 is the Avogadro number (/mol), ε is the mixed solvent dielectric constant (C^2/J·m), T is temperature (K), and a is the Debye–Hückel distance of the closest approach of ions (m). The combinatorial term (entropic term) in Eq. (26), $\ln\gamma_i^C$, represents the deviation from ideality due to differences in size and shape. The residual term (enthalpic term) in Eq. (26), $\ln\gamma_i^R$, represents the short-range energetic interactions. The activity coefficients of the combinatorial and residual terms are given below:

$$\ln\gamma_k^C = \ln\frac{\Phi_k}{x_k} + 1 - \frac{\Phi_k}{x_k} - \frac{z}{2}q_k\left(\ln\frac{\Phi_k}{\theta_k} - \frac{\Phi_k}{\theta_k} + 1\right) \quad (32)$$

$$\ln\gamma_k^R = q_k(1 - \ln S_k - A_k) \quad (33)$$

$$\ln\gamma_l^{*,C} = \ln\frac{\Phi_l}{x_l} - \frac{\Phi_l}{x_l} - \ln\frac{r_l}{r_w} + \frac{r_l}{r_w} - \frac{z}{2}q_l\left(\ln\frac{\Phi_l}{\theta_l} - \frac{\Phi_l}{\theta_l} - \ln\frac{r_l q_w}{r_w q_l} + \frac{r_l q_w}{r_w q_l}\right) \quad (34)$$

$$\ln\gamma_l^{*,R} = q_l[-\ln S_l - A_l + \ln\Psi_{wl} + \Psi_{wl}] \quad (35)$$

$$\Phi_j = \frac{r_j x_j}{\sum_i r_i x_i} \quad (36)$$

$$\Theta_j = \frac{q_j x_j}{\sum_i q_i x_i} \quad (37)$$

$$S_j = \sum_i \Theta_i \Psi_{ij} \quad (38)$$

$$A_j = \sum_i \frac{\Theta_i \Psi_{ij}}{S_i} \quad (39)$$

$$\Psi_{ji} = exp(-\frac{\tau_{ji}}{T}) \quad (40)$$

where γ_k^C is the combinatorial activity coefficient of solvent k (-), γ_k^R is the residual activity coefficient of solvent k (-), $\gamma_l^{*,C}$ is the combinatorial activity coefficient of the solute and ion l (-), $\gamma_l^{*,R}$ is the residual activity coefficient of the solute and ion l (-), Φ is the UNIQUAC average segment fraction (-), Θ is the UNIQUAC average area fraction (-), z is the lattice

coordination number (-), q is the UNIQUAC pure component area parameter (-), r is the UNIQUAC pure component volume parameter (-), S and A are the UNIQUAC parameters (-), and Ψ is the UNIQUAC interaction function (-). In Eq. (32)–(40), subscripts i and j refer to all the components, k refers to the solvent, l refers to both the solute and ion, and w refers to H_2O. The formation of an ion pair should be considered while calculating the activity coefficient of the residual term. The UNIQUAC parameter related to the surface area of the ion pairs can be calculated using the following relationships:

$$q_{z_a c, z_c a} = z_a q_c + z_c q_a \tag{41}$$

$$\theta_{z_a c, z_c a} = \theta_a \frac{z_c x_c}{\sum_{c'} z_{c'} x_{c'}} + \theta_c \frac{z_a x_a}{\sum_{a'} z_{a'} x_{a'}} \tag{42}$$

$$\langle \ln \gamma_c^{*,R} \rangle = \sum_a \left(\frac{\theta_{z_a c, z_c a}}{\sum_{a'} \theta_{z_{a'} c, z_c a}} \right) \ln \left(\gamma_c^{*,R} \right)_a \tag{43}$$

$$\langle \ln \gamma_a^{*,R} \rangle = \sum_c \left(\frac{\theta_{z_a c, z_c a}}{\sum_{c'} \theta_{z_a c', z_{c'} a}} \right) \ln \left(\gamma_a^{*,R} \right)_c \tag{44}$$

where the angular bracket represents the average value. The interaction binary parameter of τ_{ij} (−) in Eq. (40) can be expressed as follows:

$$\tau_{ij} = a_{ij} + b_{ij} T \tag{45}$$

The UNIQUAC pure component area parameters and volume parameters, q and r, are listed in Table 4. Detailed information on the electrolyte UNIQUAC model used in this study is included in a previous paper [46] and the Supporting Information.

3.3. Parameter regression

The symmetric mean absolute percentage error (SMAPE) method was used to compare the experimental data and the predicted values using the electrolyte UNIQUAC model. In the case of the SMAPE method, since the denominator cannot be 0, it is possible to prevent the error value from becoming illogically large.

$$\text{SMAPE} = \frac{100}{n} \sum_{i=1}^{n} \left| \frac{A_i - C_i}{(A_i + C_i)/2} \right| \tag{46}$$

where A_i is the actual value, C_i is the calculated value, and n is the number of data. The binary parameters (τ_{ij}) of the electrolyte UNIQUAC model were regressed to minimize the SMAPE. An in-house MATLAB model was used to solve the equilibrium equation, thermodynamic model (electrolyte UNIQUAC), and parameter regression.

4. Results and discussion

4.1. Experimental data of CO_2 solubility

The solubility of CO_2 in the DIPA and MDEA aqueous amine solutions was measured to validate the experimental method and data in the temperature range of 313.15–393.15 K. The results of the experimental data on CO_2 solubility are compared in Figs. 1 and 2. Fig. 1 shows a comparison of CO_2 solubility in 20–30 wt% MDEA and 80–70 wt% H_2O at 313.15–393.15 K between the results obtained in the present work and those reported the literature [14,65–68]. The experimental CO_2 solubility data obtained herein were in good agreement with the published data reported by Baek and Yoon [65] and Shen and Li [66] using a 30 wt% MDEA aqueous solution. In addition, the experimental CO_2 solubility in the 20 wt% MDEA aqueous solution was very close to the published data reported by Bhairi [67], Rho et al. [14], and Jou et al. [68]. In addition, the CO_2 solubility in 30–45 wt% DIPA and 70–55 wt% H_2O at 298.15–313.15 K between the results obtained in the present work and those reported in the literature [13,54,69] are compared. Fig. 2 shows that the experimental CO_2 solubility data obtained herein were also in good agreement with the data reported by Isaacs et al. [13], Haghtalab et al. [54], and Dell'Era et al. [69]. The experimental CO_2 solubility and associated uncertainty in the single-amine aqueous solutions, DIPA and MDEA in this study, are shown in the Supporting Information.

In the case of blended DIPA and MDEA aqueous amine solutions, very little experimental data on CO_2 solubility have been reported to date. Jenab et al. [15] measured CO_2 solubility in a blended DIPA and MDEA aqueous solution at 313.15–343.15 K. Vahidi et al. [12] reported the experimental data and modeling of CO_2 solubility in blended DIPA and MDEA aqueous solution at 313.2–358.2 K using Deshmukh–Mather model. To overcome the MDEA's weakness, DIPA was used in small amounts. In the present work, CO_2 solubility in the blended DIPA and MDEA aqueous solutions was measured using various blending ratios under the wide range of temperature, absorption condition (323.15 K) and desorption condition (383.15 K). The weight percent of water and total amine were fixed to 70 wt% and 30 wt% and the mixing ratios (weight ratios) of DIPA and MDEA were set to 3:7, 5:5, and 7:3. Accordingly, the weight percent of DIPA:MDEA:H_2O were 9:21:70, 15:15:70 and 21:9:70 (wt.%), respectively. Table 5 shows the CO_2 solubility data, CO_2 partial pressure (P/kPa), according to the loading ratio in Eq. (1) in the blended amine solutions at 323.15–383.15 K with the uncertainty. At low temperatures, the higher the mass fraction of MDEA, the higher the CO_2-loading ratio, whereas at high temperatures, the higher the mass fraction of DIPA, the higher the CO_2-loading ratio under the same CO_2 partial pressure.

Table 4
UNIQUAC volume and surface area parameters obtained for component k.

Component k	r_k	q_k	reference
DIPA	5.63744	4.796	ASPEN databank V11
MDEA	4.2624	3.42	Al-Rashed and Ali [46]
H_2O	0.92	1.4	Abrams and Prausnitz [47]
CO2	1.3	1.12	Abrams and Prausnitz [47]
$DIPAH^+$	5.6	4.7	This work
$MDEAH^+$	4.2	3.4	This work
H_3O^+	0.92	1.4	This work
OH^-	0.92	1.4	This work
CO_3^{-2}	1.2459	1.12	This work
HCO_3^-	1.2459	1.12	This work
$DIPACOO^-$	6.63944	5.676	This work

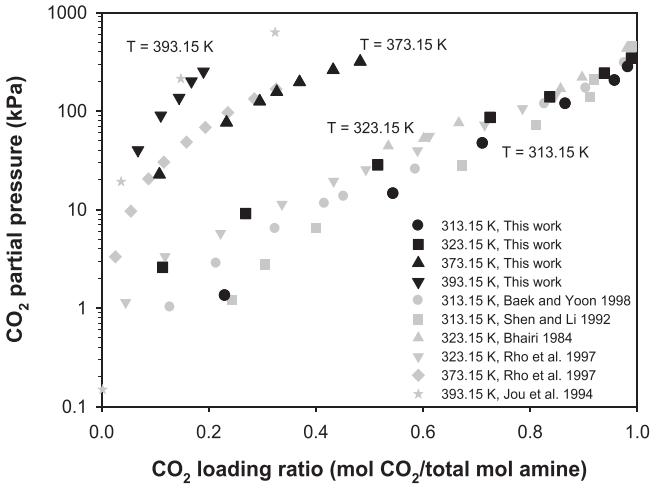

Fig. 1. A comparison of the experimental CO_2 solubility data obtained in aqueous solutions of MDEA: (●, ●, ■) 30 wt% MDEA, (■, ▲, ▼, ▲,▼,◆,★) 20 wt% MDEA .

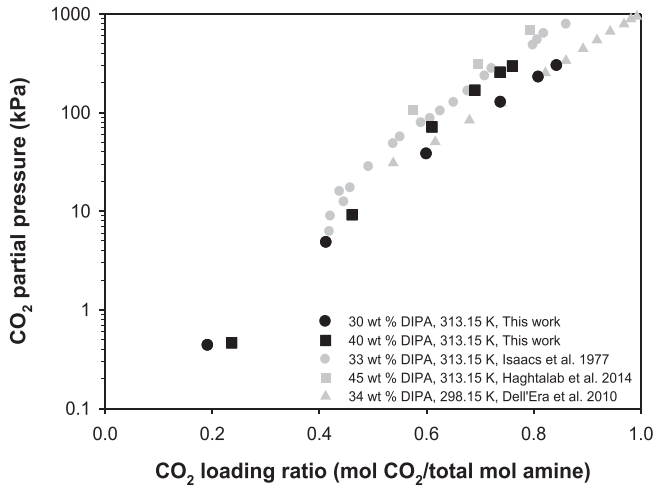

Fig. 2. A comparison of the experimental CO_2 solubility data obtained in aqueous solutions of DIPA: (●, ■) This work, (●) Isaacs et al. (1977), (■) Haghtalab et al. (2014), (▲) Dell'Era et al. (2010).

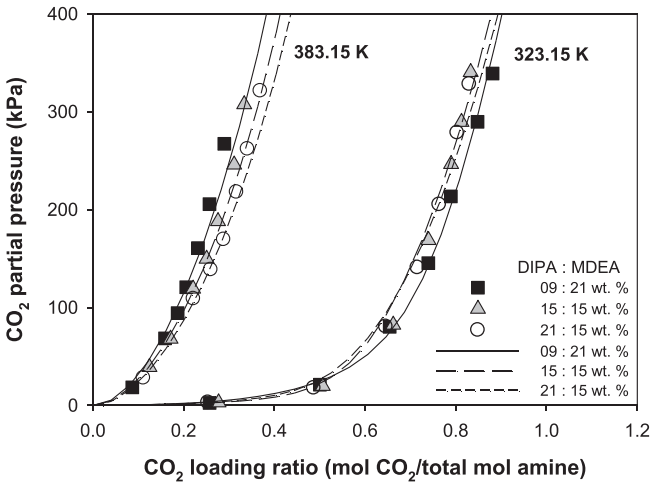

Fig. 3. CO_2 partial pressure as a function of the CO_2-loading ratio for the DIPA–MDEA–H_2O system. Experimental data (point) and model prediction obtained using the electrolyte UNIQUAC model (line) according to the blending ratio of DIPA and MDEA (H_2O balanced, 70 wt%).

Table 5
Experimental data of CO_2 partial pressure in DIPA + MDEA + H_2O[a] with uncertainty.

$T = 323.15$ K			$T = 383.15$ K		
α	P/kPa	uncertainty	α	P/kPa	uncertainty
9 wt% DIPA:21 wt% MDEA					
0.257	2.538	0.00310	0.074	40.837	0.00393
0.500	21.438	0.00160	0.143	95.533	0.00632
0.654	81.354	0.00026	0.170	122.600	0.00307
0.740	147.299	0.00732	0.191	147.341	0.00785
0.789	216.380	0.00434	0.223	177.899	0.00639
0.848	293.612	0.00399	0.251	218.374	0.00919
0.881	343.573	0.00167	0.286	277.825	0.01773
$T = 323.15$ K			$T = 383.15$ K		
α	P/kPa	uncertainty	α	P/kPa	uncertainty
15 wt% DIPA:15 wt% MDEA					
0.277	3.081	0.00130	0.116	53.647	0.01091
0.507	20.082	0.00458	0.163	87.964	0.01123
0.662	83.515	0.00150	0.221	126.794	0.03383
0.740	171.004	0.00965	0.250	158.815	0.00880
0.790	249.793	0.00748	0.284	185.691	0.01246
0.813	293.363	0.00914	0.333	223.146	0.01154
0.833	344.952	0.00367	0.368	266.569	0.00786
$T = 323.15$ K			$T = 383.15$ K		
α	P/kPa	uncertainty	α	P/kPa	uncertainty
21 wt% DIPA:9 wt% MDEA					
0.254	3.069	0.00536	0.104	40.508	0.00431
0.487	17.991	0.00056	0.219	114.447	0.01008
0.646	81.627	0.00558	0.255	148.534	0.01007
0.716	142.641	0.00410	0.283	179.743	0.01152
0.764	207.897	0.00353	0.327	205.817	0.01660
0.803	282.307	0.00716	0.363	232.432	0.01779
0.830	332.572	0.00370	0.395	287.589	0.00564

[a] CO_2 loading α = (mol of CO_2/total mol of amine), H_2O balanced (70 wt%).

4.2. Modeling and simulation

In this study, the experimental data (points) and the calculated CO_2 partial pressure obtained using the electrolyte UNIQUAC model (lines) were compared. The CO_2 partial pressures at 323.15 K (absorption condition) and 383.15 K (desorption condition) for DIPA and MDEA blended amine aqueous systems are shown in Fig. 3 (a) and (b), respectively. Fig. 4 shows the parity plot between the experimental and estimated values of the CO_2 partial pressure with the SMAPE level. In most cases, the predicted CO_2 partial pressures obtained using the electrolyte UNIQUAC model are in good agreement with the experimental data. Fig. 3 shows that the electrolyte UNIQUAC model describes

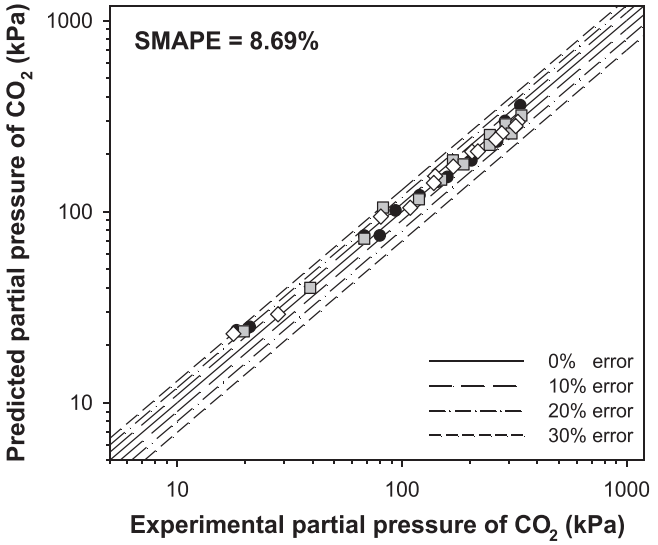

Fig. 4. Parity plots for the experimental data and simulated results obtained for the partial pressure of CO_2 in DIPA and MDEA blended amine solutions over the entire temperature range studied (●: 9 wt% DIPA, 21 wt% MDEA; ■: 15 wt% DIPA, 15 wt% MDEA; ◇: 21 wt% DIPA, 9 wt% MDEA).

the experimental data well at low temperature (323.15 K) rather than at high temperature (383.15 K). The obtained SMAPE value for each amine blending ratio, 9:21, 15:15, and 21:9 wt% of DIPA and MDEA, were 10.68%, 7.70%, and 7.67%. The electrolyte UNIQUAC model predicted experimental data well as the blending ratio of DIPA was low. However, The SMAPE level of all the 42 experimental data were 8.69% over a wide range of temperatures (323.15–383.15 K) and CO_2 partial pressures (2.5–345 kPa). The model developed in this study can be applied sufficiently to a wide temperature range and various blending ratio of amine.

4.3. Mole fraction and pH changes in the liquid phase

To estimate the mole fraction of all species (four molecules and seven electrolytes) in the liquid phase, six equilibrium expressions, four mass balances, and one electroneutrality must be solved simultaneously. In this study, the molar fractions were calculated using the successive (iterative) substitution method [39] with extremely low relative

tolerances ($<10^{-7}$). Fig. 5 represents the liquid-phase mole fraction of 10 components (three molecules, three cations, and four anions) except H_2O in the 15:15 wt% of the DIPA and MDEA blended amine system at 323.15 K. Although the molar fractions of some ions such as OH^-, H_3O^+, and CO_3^{2-} in the liquid phase are extremely low, the molar fractions of all 11 species must be calculated very accurately in order to calculate the pH and molar fractions of the remaining species in the aqueous solution. In addition, Fig. 5 shows that most of the chemical species in the liquid phase participate in determining the CO_2-solubility behavior. In the loading ratio range of 0–0.5, increasing the loading ratio of CO_2 led to a decrease in the molar fractions of DIPA and MDEA and an increase in the molar fractions of the carbamate and bicarbonate ions. $DIPACOO^-$ increased very rapidly, whereas HCO_3^- and $DIPAH^+$ increased gradually in the CO_2-loading ratio range of 0–0.5. However, the molar fraction of $DIPACOO^-$ decreased slightly in the loading ratio range of 0.5–1.0, and $DIPAH^+$ increases more rapidly. In the loading ratio range of 0.7–1.0, CO_2 could no longer react, and the molar fraction of CO_2 in the liquid phase started to increase. The molar fraction of CO_3^{2-} was almost the same in the loading ratio range of 0.0–1.0. Prior to the absorption of CO_2, the mole fraction of OH^- was much higher than that of H_3O^+ because of the basicity of the amines. When the CO_2-loading ratio increased, the concentration of H_3O^+ increased and the pH decreased.

Fig. 6(a) shows the pH change with the CO_2-loading ratio using each amine blending ratio studied (9:21, 15:15, and 21:9 wt% of DIPA and MDEA). In addition, Fig. 6(b) shows the change in the pH with the blending ratio of DIPA and MDEA under the absorption (323.15 K, P_{CO_2} = 15kPa) and desorption (383.15 K, P_{CO_2} = 100kPa) conditions, respectively. An accurate calculation of the H_3O^+ concentration, such as the molar fraction of H_3O^+ in Fig. 5, is required for predicting the pH inside the reactor and designing the CO_2 absorption process. The molar fraction of H_3O^+ and the as-obtained activity coefficients were used to calculate the pH using Eq. (47).

$$\mathrm{pH} = -log_{10}\left(x_{H_3O^+} \cdot \gamma_{H_3O^+}\right) \tag{47}$$

In most cases, the higher the blending ratio of DIPA, the weaker the basicity of the blended amine aqueous solution. Fig. 6(a) shows that the pH decreases rapidly when the CO_2-loading ratio is lower than 0.1, which then decreases slightly when this ratio becomes greater than 0.1. Fig. 6(b) shows that when the blending ratio of DIPA was < 18 wt% (12 wt% of MDEA), further increasing the mass fraction of DIPA decreases the pH. At larger than 18 wt% of DIPA, the pH was almost the same when the blending ratio of DIPA increases. In the CO_2-loading ratio range of 0–1.0, the pH range was approximately 11.9–9.0 (Fig. 6(a)). If the system is under the absorption and desorption conditions, the pH range was determined to be 10.6–10.0 and 10.2–9.9 using the various blending ratios of DIPA and MDEA, respectively (Fig. 6(b)).

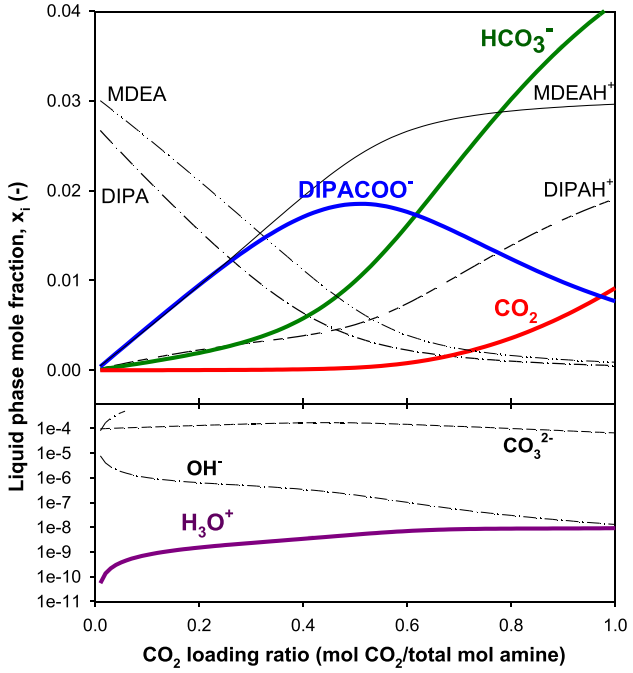

Fig. 5. Model-predicted liquid phase concentration of each species of *i* for 15 wt% DIPA and 15 wt% MDEA blended amine (H_2O balanced, 70 wt%) at 323.15 K.

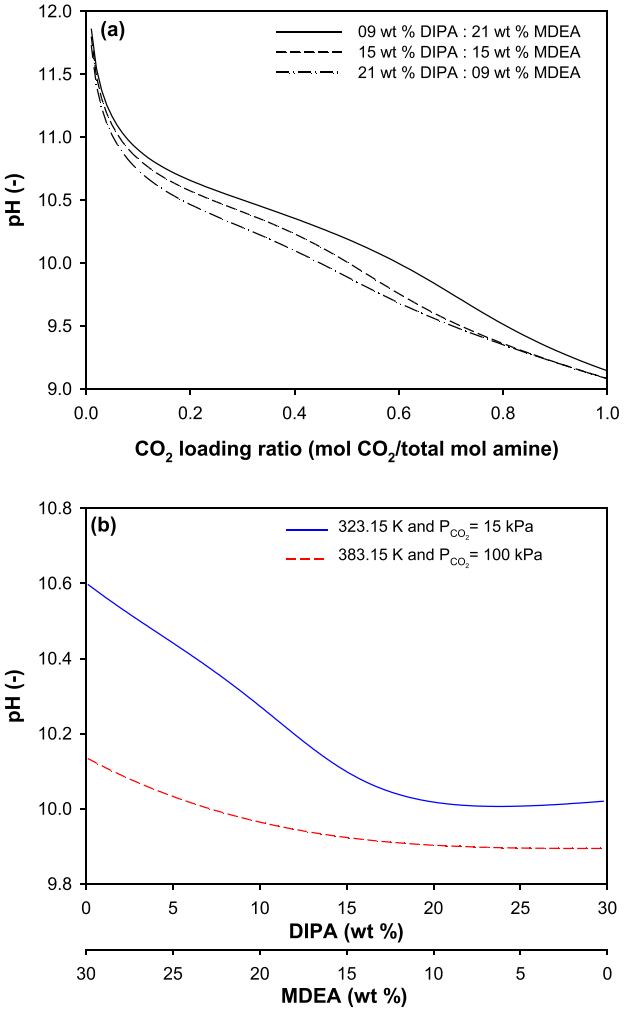

Fig. 6. Predicted pH changes according to the (a) CO_2-loading ratio in 9:21, 15:15, and 21:9 wt% DIPA and MDEA blended aqueous solutions (H_2O balanced, 70 wt%) at 323.15 K and (b) blend ratio under the absorption (323.15 K, P_{CO_2}= 15 kPa) and desorption (383.15 K, P_{CO_2}= 100 kPa) conditions.

4.4. Behavior of carbamate and bicarbonate

The liquid phase composition, such as the molar fractions of hydronium (H_3O^+), bicarbonate (HCO_3^-), and carbamate ($DIPACOO^-$) ions, was affected by the loading ratio of CO_2, as shown in Fig. 5. CO_2 dissolves in water and reacts with H_2O to form bicarbonate, as shown in Eq. (4). In addition, carbamate was formed upon the reaction with bicarbonate and carbamate, as shown in Eq. (9). Therefore, the behaviors of bicarbonate and carbamate ions provide important information for predicting CO_2 solubility in DIPA and MDEA blended amine aqueous

systems. In this section, the effects of the blending ratio and temperature on the liquid-phase mole fractions for the above ions, carbamate and bicarbonate ions, have been discussed under the absorption and desorption conditions. It is assumed that the absorption conditions are $T = 323.15$ K, $P_{CO_2} = 15$kPa and the desorption conditions are $T = 383.15$ K, and $P_{CO_2} = 100$kPa [70].

Fig. 7(a) and (b) show the molar fractions of $DIPACOO^-$ and HCO_3^- at $P_{CO_2} = 15$kPa (blue line) and $P_{CO_2} = 100$kPa (red line) in the temperature range 313–383 K according to different blending ratios (9:21, 15:15, and 21:9 wt% of DIPA and MDEA). Fig. 7(a) shows that when the partial pressure of CO_2 was 15 kPa, the molar fraction of $DIPACOO^-$ decreased as the temperature increased. However, the molar fraction of $DIPACOO^-$ slightly increases in the temperature range 313–323 K and decreases after 323 K at $P_{CO_2} = 100$kPa. The molar fraction of carbamate was higher under the absorption conditions ($P_{CO_2} = 15$kPa) compared to that under the desorption conditions ($P_{CO_2} = 100$kPa) in the low-temperature range 313–323 K. At high temperatures, the molar fraction of carbamate is lower at $P_{CO_2} = 15$kPa compared to that observed at $P_{CO_2} = 100$kPa. This opposite phenomenon is consistent with the result observed for the decreasing molar fraction of $DIPACOO^-$ when the CO_2-loading ratio was greater than 0.5, as shown in Fig. 5. The behavior of HCO_3^- was slightly different from that of $DIPACOO^-$ shown in Fig. 7(b). When the partial pressure of CO_2 was 15 kPa, the molar fraction of HCO_3^- decreased as the temperature increased. In addition, the molar fraction of HCO_3^- decreases when the temperature is increased at $P_{CO_2} = 100$kPa. The molar fraction of HCO_3^- was higher at $P_{CO_2} = 100$kPa than at $P_{CO_2} = 15$kPa.

Fig. 8 shows the model-estimated molar fraction of carbamate and bicarbonate ions according to the blending ratio of DIPA and MDEA under the absorption (323.15 K, $P_{CO_2} = 15$kPa) and desorption (383.15 K, $P_{CO_2} = 100$kPa) conditions. The molar fractions of both carbamate and bicarbonate ions are higher under the absorption conditions compared to those under the desorption conditions. When the mixing ratio of MDEA was higher than that of DIPA, no carbamate ions were formed because MDEA contains the tertiary amine. As the blending ratio of DIPA increases, the molar fraction of the carbamate also increases. The molar fraction of $DIPACOO^-$ reached its maximum value at 16.7 wt % of DIPA (13.3 wt% of MDEA) under the absorption conditions and 22.3 wt% of DIPA (7.7 wt% of MDEA) under the desorption conditions. Thereafter, the mole fraction of the formed carbamate decreased in the low-temperature region, and the value was maintained in the high-temperature region. However, in the case of bicarbonate, when the blending ratio of DIPA and MDEA is increased, the molar fraction of the bicarbonate formed first decreases and then slightly increases at the blending ratio of a specific point. The molar fraction of $DIPACOO^-$ reached its minimum at a 21.4 wt% blending ratio of the DIPA (8.6 wt% of MDEA) under the absorption conditions and 15.1 wt% of DIPA (14.9 wt% of MDEA) under the desorption conditions.

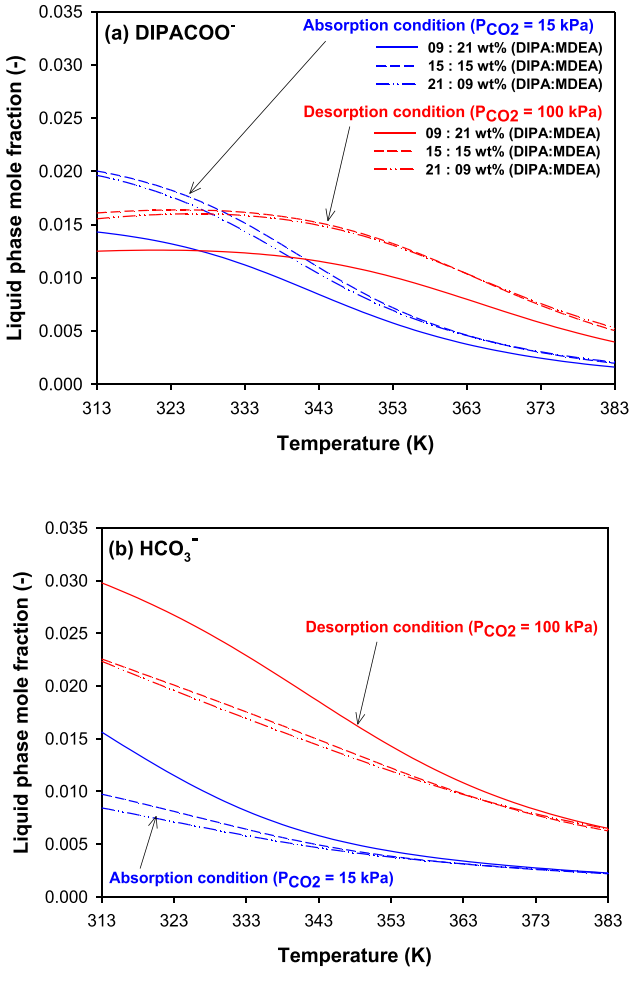

Fig. 7. Effect of temperature on the liquid phase concentration of (a) carbamate ($DIPACOO^-$) and (b) bicarbonate (HCO_3^-) according to the blending ratio of DIPA and MDEA (9:21, 15:15, and 21:9 wt% DIPA and MDEA, H_2O balanced, 70 wt%) under the absorption (P_{CO_2}= 15 kPa) and desorption (P_{CO_2}= 100 kPa) conditions.

4.5. Heat of absorption

The heat of CO_2 absorption is also important for estimating the regeneration energy required in the CO_2-absorption process. Kim et al. [22,38,71] reported the experimental and model-predicted values for the heat of CO_2 absorption in MDEA using various thermodynamic models. Zhong and Chen [53] and Ojala et al. [72] reported the experimental and model-estimated heats of absorption of CO_2 in DIPA using the electrolyte NRTL model. In the present study, the heat of absorption was calculated for various blending ratios of DIPA and MDEA using the electrolyte UNIQUAC model. The heat of CO_2 absorption can be estimated using the Gibbs–Helmholtz relationship shown below:

$$\frac{-\Delta H_{abs,CO_2}}{R} = \left[\frac{dlnP_{CO_2}}{d(1/T)}\right]_{q_{CO_2}} \quad (48)$$

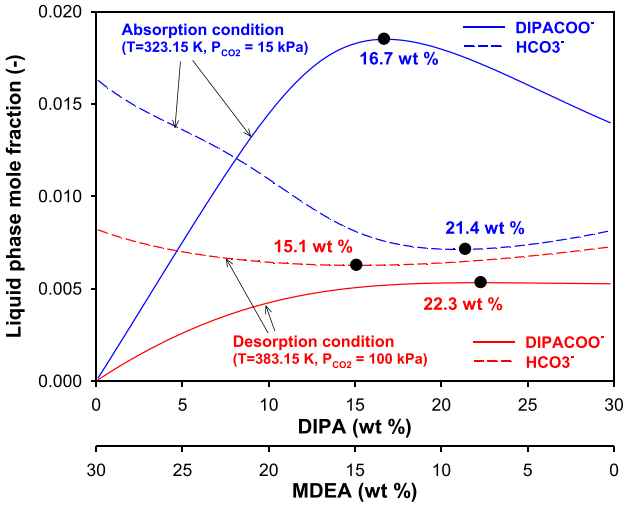

Fig. 8. Effect of the blending ratio of DIPA and MDEA (H_2O balanced, 70 wt%) on the liquid phase concentration of carbamate ($DIPACOO^-$) and bicarbonate (HCO_3^-) under the absorption (323.15 K, P_{CO_2}= 15 kPa) and desorption (383.15 K, P_{CO_2}= 100 kPa) conditions.

Several research groups including Mathers group [73] and Sdvendsen group [22,38,71,74] reported that the most reliable heat of absorption can be obtained only by measuring with a calorimetry. When calculating the heat of absorption by applying the absorption equilibrium data according to temperature to the Gibbs–Helmholtz equation, the accuracy is significantly lowered. However, in this study, in order to evaluate the effect of the blending ratio of alkanolamines on the heat of absorption, it had to be calculated by applying the predicted values of absorption equilibrium to the above equation.

Fig. 9(a) shows the heat of CO_2 absorption based on the CO_2-loading ratio at each amine blending ratio studied (9:21, 15:15, and 21:9 wt% of DIPA and MDEA). Fig. 9(b) shows the heat of CO_2 absorption based on the blending ratio of DIPA and MDEA under the absorption (323.15 K, P_{CO_2} = 15kPa) and desorption (383.15 K, P_{CO_2} = 100kPa) conditions, respectively. Fig. 9(a) shows that the heat of absorption changes sharply in the CO_2-loading ratio range of 0.4–0.7 in the presence of 15:15 and 21:9 wt% of DIPA and MDEA blended amine solutions. In contrast, at 9:21 wt%, the heat of absorption decreases rapidly in the CO_2-loading ratio range of 0.2–0.4 and 0.7–0.8 for DIPA and MDEA blended amine solutions, respectively. When the CO_2-loading ratio range was 0.18–0.42, the heat of absorption at 9:21 wt% was slightly lower than that at 15:15 and 21:9 wt%. The heat of absorption was predicted to be higher at 9:21 wt% than at the other two blending ratios at a loading ratio of greater than 0.51. In the CO_2-loading ratio range of 0.0–1.0, for a given blending ratio, the heat of absorption was approximately in the range 1.3–49.7 kJ/mol CO_2. In the 9:21, 15:15, and 21:9 wt% of DIPA and MDEA blended amine solutions, the maximum values observed for the heat of CO_2 absorption were 46.0, 49.7, and 45.4 kJ/mol CO_2, respectively. Fig. 9(b) shows that the heat of absorption was in the range 48–65 kJ/mol CO_2 depending on the blending ratio of DIPA and MDEA used. Under the absorption conditions (323.15 K, P_{CO_2} = 15kPa), the maximum value observed for the heat of absorption was 65.3 kJ/mol CO_2 with a blending ratio of 11.6:18.4.% DIPA and MDEA, while that under desorption conditions (383.15 K, P_{CO_2} = 100kPa) was 62.1 kJ/mol CO_2 with a blending ratio of 15.4:14.6 wt% DIPA and MDEA.

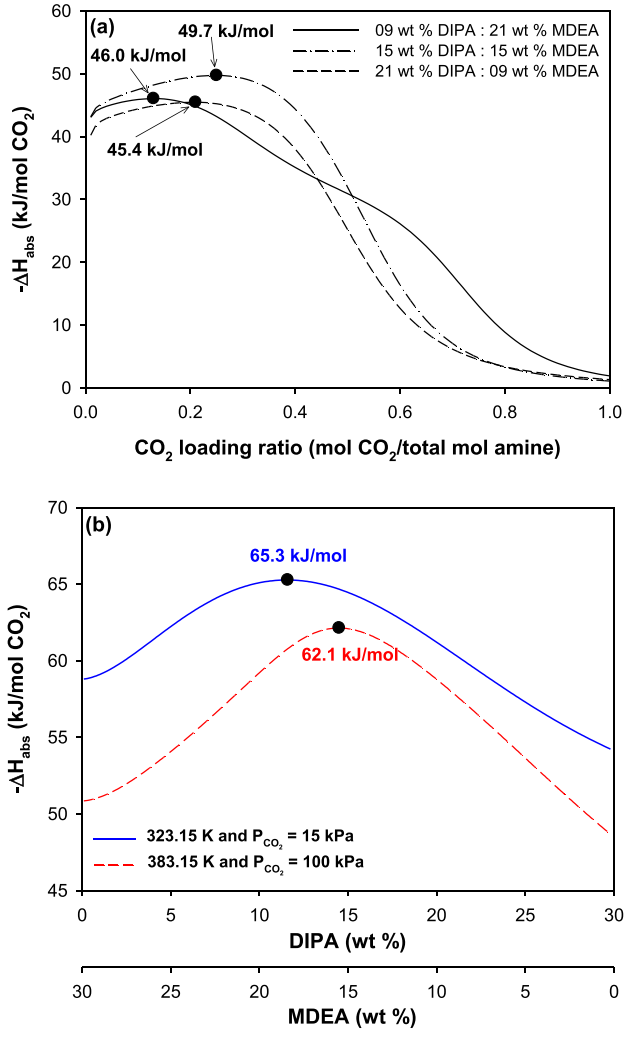

Fig. 9. Predicted heat of absorption: (a) Effect of the CO_2-loading ratio in 9:21, 15:15, and 21:9 wt% DIPA and MDEA blended aqueous solutions (H_2O balanced, 70 wt%) at 323.15 K and (b) effect of the blending ratio of DIPA and MDEA (H_2O balanced, 70 wt%) under the absorption (323.15 K, P_{CO_2}= 15 kPa) and desorption (383.15 K, P_{CO_2}= 100 kPa) conditions.

4.6. Cyclic capacity of CO_2

The sensible heat loss occurs when the rich and lean amine solvent is heat exchanged during the CO_2 absorption–desorption process. To reduce the sensible-heat loss, the solvent should have a high cyclic capacity of CO_2. In general, the cyclic capacity ($\Delta\alpha$) is defined as the difference between the CO_2 concentration in the rich and lean solutions as follows [70].

$$\Delta\alpha = \alpha_{rich} - \alpha_{lean} \tag{49}$$

Therefore, cyclic capacity is typically used when experimentally expressing degradation and oxidation characteristics caused by repeated use of CO_2 absorption solution during process operation. However, the definition of cyclic capacity has slightly different meanings under various process conditions. In addition, the cyclic capacity was different under each condition because different pressure and temperature conditions were applied to the CO_2 absorption process. In the present work, it was assumed that α_{rich} is observed under the absorption conditions and α_{lean} was observed under the desorption conditions. The difference in the cyclic capacity of CO_2 ($\Delta\alpha_{CO_2}$, mol CO_2/total mol amine) under the absorption and desorption conditions can be defined as follows:

$$\Delta\alpha_{CO_2} = \alpha_{CO_2}(T_{abs}, P_{CO_2} = 15kPa) - \alpha_{CO_2}(T_{des}, P_{CO_2} = 100kPa) \tag{50}$$

where T_{abs} is the temperature of the absorption conditions (313.15–333.15 K) and T_{des} is the temperature of the desorption conditions (373.15–393.15 K). Here, the cyclic capacity of CO_2 ($\Delta\alpha_{CO_2}$) was calculated under the absorption and desorption conditions using the DIPA and MDEA blending ratios studied (0–30:30–0 wt% DIPA and MDEA, 70 wt% H_2O).

Fig. 10 shows the cyclic capacity behaviors of the DIPA and MDEA blended amine solutions (70 wt% H_2O) at various temperatures of the absorption condition (313.15–333.15 K), at a constant desorption temperature (383.15 K), at a constant absorption temperature (323.15 K), and at various temperatures of the desorption condition (373.15–393.15 K). The effects of the absorption and desorption temperatures on the cyclic capacity were compared based on the reference conditions (T_{ads} = 323.15 K and T_{des} = 383.15 K), as indicated by the thick lines in Fig. 10(a) and (b). The cyclic capacity of CO_2 increases as the absorption temperature decreases or as the desorption temperature increases because the CO_2 absorption reaction is exothermic. When DIPA and MDEA were mixed to prepare the new blended absorbent, the optimal points (●) of the blending ratio, in which the cyclic capacity has a maximum value, can be estimated. Fortunately, for the DIPA and MDEA blended aqueous solutions, it was confirmed that an optimal blending ratio exists when the cyclic capacity is calculated from an equilibrium viewpoint. Fig. 10(a) shows the lower the absorption temperature, the smaller the mass ratio of DIPA and the larger the mass ratio of MDEA, the maximum CO_2 cyclic capacity was observed. The optimal range for the DIPA mass ratio was 10.2–14.2 wt% and for MDEA was

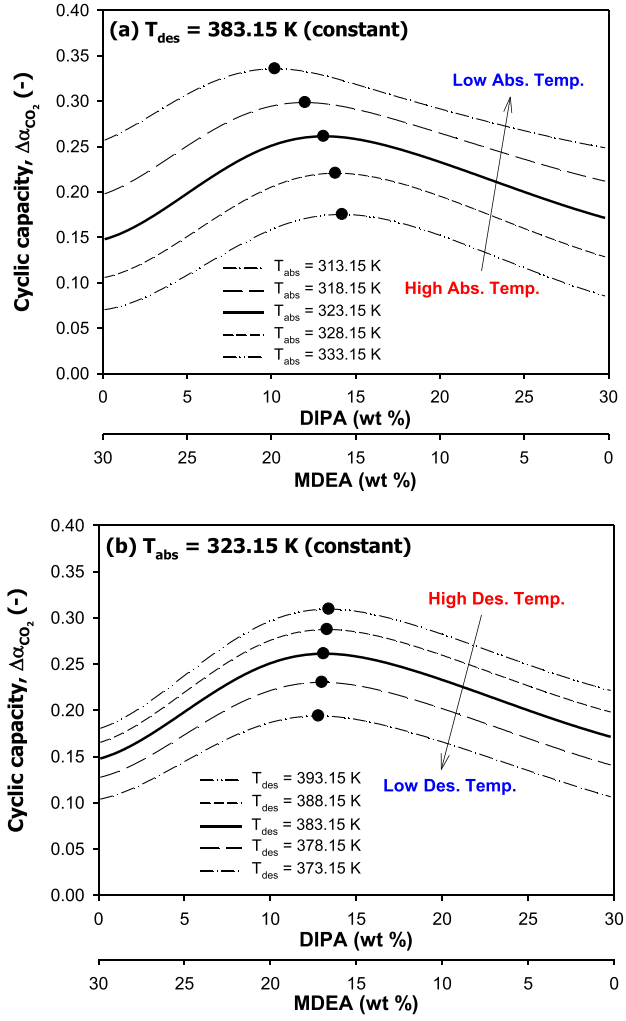

Fig. 10. Effect of the blending ratio of DIPA and MDEA on the CO_2 cyclic capacity ($\Delta\alpha_{CO_2}$) of the amine mass fraction at (a) various absorption temperatures (313.15–333.15 K) and a constant desorption temperature (383.15 K) and (b) various desorption temperatures (373.15–393.15 K) and constant absorption temperature (323.15 K) (●: Maximum values under each condition).

19.8–15.8 wt% when the absorption temperature was in the range of 313.15–333.15 K and the constant desorption temperature was 383.15 K. Fig. 10(b) shows decreasing the desorption temperature decreases the blending ratio of DIPA, exhibiting the maximum CO_2 cyclic capacity. The DIPA mass ratio range with the maximum cyclic capacity is 12.8–13.4 wt% with 17.2–16.6 wt% of MDEA at a constant absorption temperature of 323.15 K and a desorption temperature in the range of 373.15–393.15 K. The cyclic capacity of CO_2, which is defined in Eq. (50), was in the range of 0.07–0.34 when using various amine blending ratios. This simulation results were consistent with that shown in Fig. 3 (a) and (b). When the cyclic capacity of CO_2 based on the blending ratio of DIPA and MDEA was considered, it was more advantageous to use 10–15 wt% of DIPA. The above results were obtained only in terms of equilibrium. To obtain more accurate information about the cyclic capacity, more experiments, kinetics, mass transfer, modeling, etc. should be studied.

4.7. Effect of the mixing ratio of DIPA, MDEA, and H_2O

The effect of the mixing ratio used in the DIPA–MDEA–H_2O ternary system on the solubility of CO_2 was investigated. The behavior of the cyclic capacity of CO_2, heat of absorption, and pH were predicted for various mixing ratios of DIPA, MDEA, and H_2O using the triangular diagrams. The three axes represent the weight ratio of each liquid amine component (DIPA: 0–0.4; MDEA: 0–0.4; H2O: 1.0–0.6; total: 1). The spectrum and contour in the diagram represent the values of pH, heat of absorption, and cyclic capacity.

Fig. 11 shows the triangular pH diagram obtained for the various blending ratios of DIPA (0–0.4), MDEA (0–0.4), and H_2O (0.6–1.0, 100 wt% balanced) under the absorption (323.15 K, P_{CO_2} = 15kPa) and desorption (383.15 K, P_{CO_2} = 100kPa) conditions, respectively. For most of the conditions studied, the pH was higher under the absorption conditions than under the desorption conditions. The pH decreases when the mass ratio of DIPA increases or that of MDEA decreases. This result was consistent with the results shown in Fig. 6(b). When the mass ratio of H_2O increased, the pH slightly increased. Fig. 11(b) shows that the pH changes according to the mixing ratio of DIPA, MDEA, and H_2O was not significantly higher under the desorption conditions compared to that under the absorption conditions. The pH range was in the ranges 9.7–10.6 and 9.5–10.2 under the absorption and desorption conditions,

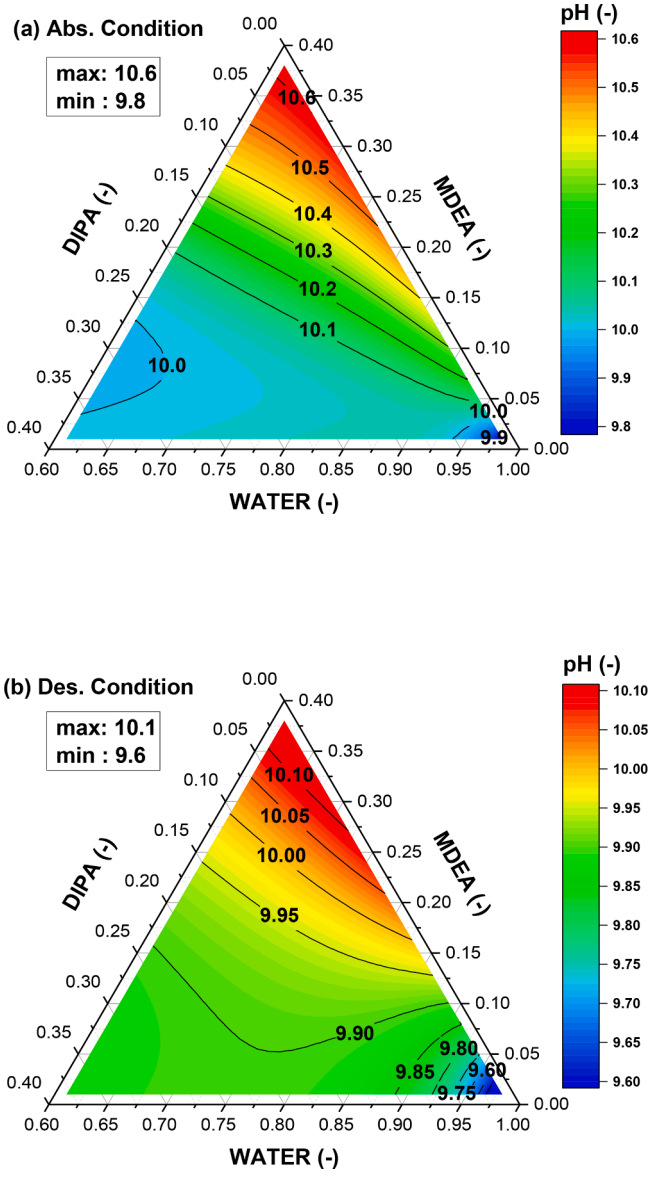

Fig. 11. Predicted pH changes using various mixing ratios (H_2O mass fraction range: 0.6–1.0, DIPA mass fraction range: 0.0–0.4, MDEA mass fraction range: 0.0–0.4) under the (a) absorption (323.15 K, P_{CO_2}= 15 kPa) and (b) desorption (383.15 K, P_{CO_2}= 100 kPa) conditions.

respectively, when using the various blending ratios of DIPA, MDEA and H_2O studied.

Fig. 12 shows the triangular heat of absorption diagram obtained for various blending ratios of DIPA (0–0.4), MDEA(0–0.4), and H_2O (0.6–1.0, 100 wt% balanced) studied under the absorption conditions (323.15 K, P_{CO_2} = 15kPa). When the blending ratio of H_2O was in the range of 0.67–1.0, the concentration of H_2O was higher and the heat of CO_2 absorption was lower. If the blending ratio of H_2O was in the range 0.6–0.9, the blending ratio with the maximum heat of absorption was observed, as shown in Fig. 9(b). The highest heat of CO_2 absorption was calculated when the blending ratio was 69:15:16 wt% of H_2O, DIPA, and MDEA. However, the lowest mixing heat was calculated when the blending ratio was 92:8:0 wt%. The heat of CO_2 absorption was in the range of 37–62 kJ/mol under the absorption conditions.

The triangular CO_2 cyclic capacity ($\Delta\alpha_{CO_2}$) diagram obtained for the various blending ratios of DIPA (0–0.4), MDEA(0–0.4), and H_2O (0.6–1.0, 100 wt% balanced) under the absorption (323.15 K, P_{CO_2} = 15kPa) and desorption (383.15 K, P_{CO_2} = 100kPa) conditions is shown in Fig. 13. When the blending ratio of DIPA was 0.05–0.4, the MDEA concentration decreased and the cyclic capacity at the same DIPA concentration reduced. The lowest point of the CO_2 cyclic capacity in the blending ratio of DIPA and H_2O was calculated at an MDEA blending ratio of<0.1. However, when the blending ratio of H_2O was in the range of 0.6–0.85, the maximum value of the cyclic capacity was predicted in the DIPA and MDEA mixture. This result was consistent with the results shown in Fig. 10. The optimal mixing ratio with the maximum cyclic capacity of CO_2 was 0.17 DIPA, 0.23 MDEA, and 0.60 H_2O. The difference in the CO_2-loading ratio between the absorption and desorption conditions, known as cyclic capacity, was in the range of 0.12–0.31. These results are predicted based on the equilibrium and simulation. For a more accurate design of the CO_2-absorption processes, the detailed properties of the blended amines, such as equilibrium, mass transfer, kinetics, corrosiveness, degradation of solvents, operability, material costs, and operating costs, must be considered using simultaneous experiments.

5. Conclusions

In this study, CO_2 solubility in blended amine aqueous solutions, DIPA and MDEA, was measured using different amine blending ratios (DIPA:MDEA = 9:21, 15:15, and 21:9 wt% and 70 wt% H_2O) and working temperatures (323.15 and 383.15 K). In addition, the effect of

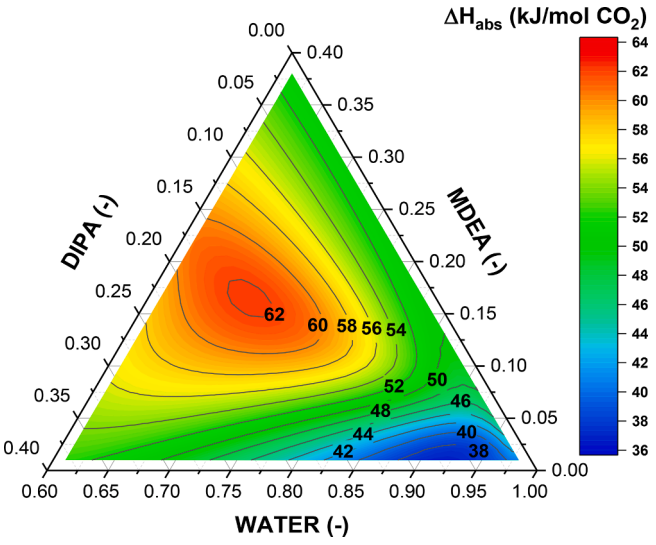

Fig. 12. Predicted heats of absorption using various mixing ratios (H_2O mass fraction range: 0.6–1.0, DIPA mass fraction range: 0.0–0.4, MDEA mass fraction range: 0.0–0.4) under the absorption conditions (323.15 K, P_{CO_2} = 15 kPa).

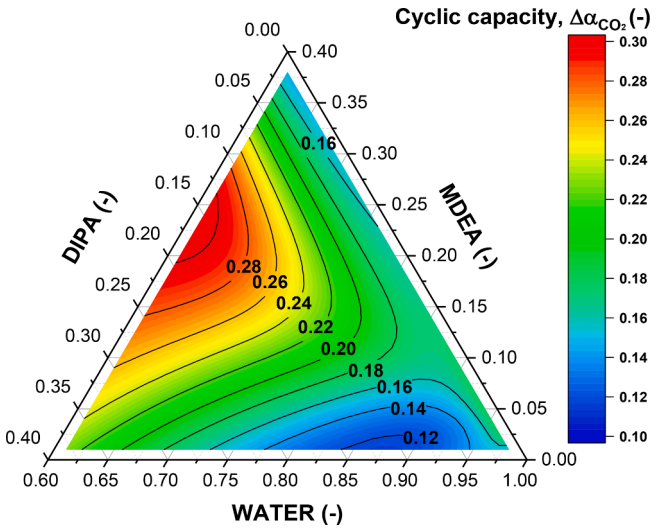

Fig. 13. Predicted cyclic capacity of CO_2 ($\Delta\alpha_{CO_2}$) using various mixing ratios (H_2O mass fraction range: 0.6–1.0, DIPA mass fraction range: 0.0–0.4, MDEA mass fraction range: 0.0–0.4) under the absorption (323.15 K, P_{CO_2}= 15 kPa) and desorption (383.15 K, P_{CO_2}= 100 kPa) conditions.

the temperature and the blending ratio of DIPA, MDEA, and H_2O was theoretically investigated under absorption/desorption conditions (323.15 K, P_{CO_2} = 15kPa and 383.15 K, P_{CO_2} = 100kPa, respectively). To predict the CO_2 absorption behavior and to calculate the mole fraction of 11 species in the liquid phase, the successive substitution method was used. 11 equations for 11 variables were solved simultaneously and accurately under extremely low relative tolerance ($<10^{-7}$). The electrolyte UNIQUAC model was introduced to consider the nonideality of the liquid phase. In the entire experimental range, the binary parameter of the electrolyte UNIQUAC model was regressed from the experiment. It was observed that the electrolyte UNIQUAC model shows a good correlation of the present experimental data with SMAPE level of 8.69%.

Using the developed models with the obtained binary parameters, the CO_2 partial pressure in the gas (vapor) phase, liquid phase concentrations for all components were estimated. Then, the behavior of the CO_2 cyclic capacity, heat of absorption, and pH were predicted for various mixing ratios of DIPA, MDEA, and H_2O using the triangular diagrams. The predicted cyclic capacity was in the range of 0.12 (Min.) – 0.31 (Max.) and the optimal mixing ratio of DIPA, MDEA and H_2O for maximum CO_2 cyclic capacity was 0.17, 0.23, and 0.60. The predicted heat of CO_2 absorption was in the range of 37 (Min.) – 62 (Max) kJ/mol under the absorption conditions. If the mass ratio of H_2O was in the range of 0.67–1.00, increasing the concentration of H_2O decreased the heat of CO_2 absorption. When the mixing ratio of H_2O is in the range of 0.60–0.90, the blending ratio of DIPA and MDEA with the maximum value of heat of absorption was calculated. The predicted pH range was 9.7–10.6 under the absorption conditions and 9.5–10.2 under the desorption conditions. If the mass ratio of H_2O was in the range of 0.67–1.0, increasing the concentration of H_2O decreased the heat of CO_2 absorption.

This paper has great significance in predicting the CO_2 absorption characteristics in the blended alkanolamine aqueous solution by applying it to a thermodynamic model, especially an electrolyte UNIQUAC model. If the results of the CO_2 solubility model developed in this work are utilized, significant information according to the amine blending ratio can be obtained for more accurate simulation and design. In addition, it will be possible to provide insights into the CO_2 solubility, pH, heat of absorption, cyclic capacity, etc. according to the blending ratio. The above results were obtained only in terms of thermodynamic equilibrium. For a more accurate calculation of the CO_2 solubility and designing CO_2 absorption processes, large-scale experiments,

equilibrium, and kinetic aspects should be considered simultaneously.

CRediT authorship contribution statement

Bong Keun Choi: Methodology, Software, Visualization, Investigation, Writing - original draft. **Seung-Mo Kim:** Software, Visualization, Investigation. **Kyung-Min Kim:** Investigation, Writing - review & editing. **Ung Lee:** Investigation, Funding acquisition. **Jeong Ho Choi:** Investigation. **Jong-Seop Lee:** Investigation, Validation, Resources. **Il Hyun Baek:** Investigation. **Sung Chang Nam:** Investigation, Supervision, Funding acquisition. **Jong-Ho Moon:** Conceptualization, Writing - review & editing, Supervision, Project administration.

Declaration of Competing Interest

The authors declare that they have no known competing financial interests or personal relationships that could have appeared to influence the work reported in this paper.

Acknowledgements

This work was supported by a National Research Foundation of Korea (NRF) grant funded by the Korean government (MSIT) (No. 2020M1A2A6079067 & 2020M3H7A1098273).

Appendix A. Supplementary data

Supplementary data to this article can be found online at https://doi.org/10.1016/j.cej.2021.129517.

References

[1] D. Zhu, M. Fang, Z. Lv, Z. Wang, Z. Luo, Selection of blended solvents for CO2 absorption from coal-fired flue gas. Part 1: Monoethanolamine (MEA)-based solvents, Energy Fuels 26 (1) (2012) 147–153.
[2] Z.(. Liang, W. Rongwong, H. Liu, K. Fu, H. Gao, F. Cao, R. Zhang, T. Sema, A. Henni, K. Sumon, D. Nath, D. Gelowitz, W. Srisang, C. Saiwan, A. Benamor, M. Al-Marri, H. Shi, T. Supap, C. Chan, Q. Zhou, M. Abu-Zahra, M. Wilson, W. Olson, R. Idem, P.(PT). Tontiwachwuthikul, Recent progress and new developments in post-combustion carbon-capture technology with amine based solvents, Int. J. Greenhouse Gas Control 40 (2015) 26–54.
[3] J.H. Choi, Y.E. Kim, S.C. Nam, S.H. Yun, Y.I. Yoon, J.-H. Lee, CO 2 absorption characteristics of a piperazine derivative with primary, secondary, and tertiary amino groups, Korean J. Chem. Eng. 33 (11) (2016) 3222–3230.
[4] A. Haghtalab, V. Gholami, Carbon dioxide solubility in the aqueous mixtures of diisopropanolamine+ l-arginine and diethanolamine+ l-arginine at high pressures, J. Mol. Liq. 288 (2019), 111064.
[5] H.A. Shirazizadeh, A. Haghtalab, Measurement and modeling of CO2 solubility in binary aqueous DMSO and MDEA and their ternary mixtures at different temperatures and compositions, Fluid Phase Equilib. 528 (2021), 112845.
[6] A. Dey, B. Mandal, S.K. Dash, Analysis of equilibrium CO2 solubility in aqueous APDA and its potential blends with AMP/MDEA for postcombustion CO2 capture, Int. J. Energy Res. 44 (15) (2020) 12395–12415.
[7] M. Xiao, H. Liu, H. Gao, Z. Liang, CO2 absorption with aqueous tertiary amine solutions: Equilibrium solubility and thermodynamic modeling, J. Chem. Thermodyn. 122 (2018) 170–182.
[8] S. Kumar, R. Padhan, M.K. Mondal, Equilibrium Solubility Measurement and Modeling of CO2 Absorption in Aqueous Blend of 2-(Diethyl amino) Ethanol and Ethylenediamine, J. Chem. Eng. Data 65 (2) (2020) 523–531.
[9] R. Mahmoodi, M. Mofarahi, A.A. Izadpanah, M. Afkhamipour, A. Hajizadeh, Experimental and Theoretical Investigation of Equilibrium Absorption Performance: Effect of Alkyl Amines as Promoters on the CO2 Loading of 2-Amino-2-methyl-1-propanol at 313 K, Energy Fuels 33 (9) (2019) 8985–8997.
[10] A.T. Zoghi, F. Feyzi, S. Zarrinpashneh, Experimental investigation on the effect of addition of amine activators to aqueous solutions of N-methyldiethanolamine on the rate of carbon dioxide absorption, Int. J. Greenhouse Gas Control 7 (2012) 12–19.
[11] E.E. Isaacs, F.D. Otto, A.E. Mather, The solubility of mixtures of carbon dioxide and hydrogen sulphide in an aqueous DIPA solution, The Can. J. Chem. Eng. 55 (2) (1977) 210–212.
[12] M. Vahidi, A.T. Zoghi, B. Moshtari, B. Nonahal, Equilibrium solubility of carbon dioxide in an aqueous mixture of N-methyldiethanolamine and diisopropanolamine: an experimental and modeling study, J. Chem. Eng. Data 58 (7) (2013) 1963–1968.
[13] E.E. Isaacs, F.D. Otto, A.E. Mather, Solubility of hydrogen sulfide and carbon dioxide in an aqueous diisopropanolamine solution, J. Chem. Eng. Data 22 (1) (1977) 71–73.
[14] S.-W. Rho, K.-P. Yoo, J.S. Lee, S.C. Nam, J.E. Son, B.-M. Min, Solubility of CO2 in aqueous methyldiethanolamine solutions, J. Chem. Eng. Data 42 (6) (1997) 1161–1164.
[15] M.H. Jenab, M. Vahidi, M. Mehrabi, Solubility of carbon dioxide in aqueous mixtures of DIPA+ MDEA and DIPA+ PZ solutions, J. Chin. Chem. Soc. 53 (2) (2006) 283–286.
[16] M.Z. Haji-Sulaiman, M.K. Aroua, A. Benamor, Analysis of equilibrium data of CO2 in aqueous solutions of diethanolamine (DEA), methyldiethanolamine (MDEA) and their mixtures using the modified Kent Eisenberg model, Chem. Eng. Res. Des. 76 (8) (1998) 961–968.
[17] M.K. Aroua, R. Mohd Salleh, Solubility of CO2 in aqueous piperazine and its modeling using the Kent-Eisenberg approach, Chem. Eng. Technol. 27 (1) (2004) 65–70.
[18] R.D. Deshmukh, A.E. Mather, A mathematical model for equilibrium solubility of hydrogen sulfide and carbon dioxide in aqueous alkanolamine solutions, Chem. Eng. Sci. 36 (2) (1981) 355–362.
[19] Y.-G. Li, A.E. Mather, Correlation and prediction of the solubility of carbon dioxide in a mixed alkanolamine solution, Ind. Eng. Chem. Res. 33 (8) (1994) 2006–2015.
[20] T.T. Teng, A.E. Mather, Solubility of H2S, CO2 and their mixtures in an AMP solution, Can. J. Chem. Eng. 67 (5) (1989) 846–850.
[21] R.H. Weiland, T. Chakravarty, A.E. Mather, Solubility of carbon dioxide and hydrogen sulfide in aqueous alkanolamines, Ind. Eng. Chem. Res. 32 (7) (1993) 1419–1430.
[22] I. Kim, K.A. Hoff, E.T. Hessen, T. Haug-Warberg, H.F. Svendsen, Enthalpy of absorption of CO2 with alkanolamine solutions predicted from reaction equilibrium constants, Chem. Eng. Sci. 64 (9) (2009) 2027–2038.
[23] A. Benamor, M.K. Aroua, Modeling of CO2 solubility and carbamate concentration in DEA, MDEA and their mixtures using the Deshmukh-Mather model, Fluid Phase Equilib. 231 (2) (2005) 150–162.
[24] R.J. Macgregor, A.E. Mather, Equilibrium solubility of H2S and CO2 and their mixtures in a mixed solvent, Can. J. Chem. Eng. 69 (6) (1991) 1357–1366.
[25] H. Pahlavanzadeh, S. Nourani, M. Saber, Experimental analysis and modeling of CO2 solubility in AMP (2-amino-2-methyl-1-propanol) at low CO2 partial pressure using the models of Deshmukh-Mather and the artificial neural network, J. Chem. Thermodyn. 43 (12) (2011) 1775–1783.
[26] P. Pakzad, et al., An experimental and modeling study of CO2 solubility in a 2-amino-2-methyl-1-propanol (AMP)+ N-methyl-2-pyrrolidone (NMP) solution, Chem. Eng. Sci. 175 (2018) 365–376.
[27] P. Pakzad, et al., Experimental data, thermodynamic and neural network modeling of CO2 absorption capacity for 2-amino-2-methyl-1-propanol (AMP)+ Methanol (MeOH)+ H2O system, J. Nat. Gas Sci. Eng. 73 (2020), 103060.
[28] C.-C. Chen, Y. Song, Generalized electrolyte-NRTL model for mixed-solvent electrolyte systems, AIChE J. 50 (8) (2004) 1928–1941.
[29] G.M. Bollas, C.C. Chen, P.I. Barton, Refined electrolyte-NRTL model: Activity coefficient expressions for application to multi-electrolyte systems, AIChE J. 54 (6) (2008) 1608–1624.
[30] C.-C. Chen, H.I. Britt, J.F. Boston, L.B. Evans, Local composition model for excess Gibbs energy of electrolyte systems. Part I: Single solvent, single completely dissociated electrolyte systems, AIChE J. 28 (4) (1982) 588–596.
[31] C.-C. Chen, L.B. Evans, A local composition model for the excess Gibbs energy of aqueous electrolyte systems, AIChE J. 32 (3) (1986) 444–454.
[32] Y. Zhang, H. Que, C.-C. Chen, Thermodynamic modeling for CO2 absorption in aqueous MEA solution with electrolyte NRTL model, Fluid Phase Equilib. 311 (2011) 67–75.
[33] D.M. Austgen, G.T. Rochelle, C.C. Chen, Model of vapor-liquid equilibria for aqueous acid gas-alkanolamine systems. 2. Representation of hydrogen sulfide and carbon dioxide solubility in aqueous MDEA and carbon dioxide solubility in aqueous mixtures of MDEA with MEA or DEA, Ind. Eng. Chem. Res. 30 (3) (1991) 543–555.
[34] D.M. Austgen, G.T. Rochelle, X. Peng, C.C. Chen, Model of vapor-liquid equilibria for aqueous acid gas-alkanolamine systems using the electrolyte-NRTL equation, Ind. Eng. Chem. Res. 28 (7) (1989) 1060–1073.
[35] M.L. Posey, G.T. Rochelle, A thermodynamic model of Methyldiethanolamine–CO2– H2S– Water, Ind. Eng. Chem. Res. 36 (9) (1997) 3944–3953.
[36] E.T. Hessen, T. Haug-Warberg, H.F. Svendsen, The refined e-NRTL model applied to CO2–H2O–alkanolamine systems, Chem. Eng. Sci. 65 (11) (2010) 3638–3648.
[37] S. Ma'mun, J.P. Jakobsen, H.F. Svendsen, O. Juliussen, Experimental and modeling study of the solubility of carbon dioxide in aqueous 30 mass% 2-((2-aminoethyl) amino) ethanol solution, Ind. Eng. Chem. Res. 45 (8) (2006) 2505–2512.
[38] I. Kim, E.T. Hessen, T. Haug-Warberg, H.F. Svendsen, Enthalpies of absorption of CO2 in aqueous alkanolamine solutions from e-NRTL model, Energy Procedia 1 (1) (2009) 829–835.
[39] J.-H. Moon, J.-S. Lee, Y.C. Park, J. Park, D.-H. Chun, J. Yoo, H.-Y. Shin, B.-M. Min, Experimental and Modeling Study of Vapor Liquid Equilibrium for a Methyldiethanolamine–CO2–H2S–Water Quaternary System Using Activity Coefficient Models with Corrected Equilibrium Constants, Energy Fuels 33 (5) (2019) 4401–4411.
[40] U.E. Aronu, S. Gondal, E.T. Hessen, T. Haug-Warberg, A. Hartono, K.A. Hoff, H. F. Svendsen, Solubility of CO2 in 15, 30, 45 and 60 mass% MEA from 40 to 120 C and model representation using the extended UNIQUAC framework, Chem. Eng. Sci. 66 (24) (2011) 6393–6406.

[41] H. Mehdizadeh, M. Gupta, E.F. Da Silva, H.F. Svendsen, Representation of Piperazine-CO2-H2O system using extended-UNIQUAC and computational chemistry, Energy Procedia 37 (2013) 1871–1880.
[42] H. Mehdizadeh, M. Gupta, I. Kim, E.F. Da Silva, T. Haug-Warberg, H.F. Svendsen, AMP–CO2–water thermodynamics, a combination of UNIQUAC model, computational chemistry and experimental data, Int. J. Greenhouse Gas Control 18 (2013) 173–182.
[43] L. Kaewsichan, O. Al-Bofersen, V.F. Yesavage, M.S. Selim, Predictions of the solubility of acid gases in monoethanolamine (MEA) and methyldiethanolamine (MDEA) solutions using the electrolyte-UNIQUAC model, Fluid Phase Equilib. 183-184 (2001) 159–171.
[44] A. Haghtalab, M. Dehghani Tafti, Electrolyte UNIQUAC– NRF model to study the solubility of acid gases in alkanolamines, Ind. Eng. Chem. Res. 46 (18) (2007) 6053–6060.
[45] A. Haghtalab, K. Peyvandi, Generalized Electrolyte-UNIQUAC-NRF model for calculation of solubility and vapor pressure of multicomponent electrolytes solutions, J. Mol. Liq. 165 (2012) 101–112.
[46] O.A. Al-Rashed, S.H. Ali, Modeling the solubility of CO2 and H2S in DEA–MDEA alkanolamine solutions using the electrolyte–UNIQUAC model, Sep. Purif. Technol. 94 (2012) 71–83.
[47] D.S. Abrams, J.M. Prausnitz, Statistical thermodynamics of liquid mixtures: a new expression for the excess Gibbs energy of partly or completely miscible systems, AIChE J. 21 (1) (1975) 116–128.
[48] B.-K. Choi, S.-M. Kim, J.-S. Lee, Y.C. Park, D.-H. Chun, H.-Y. Shin, H.-J. Sung, B.-M. Min, J.-H. Moon, Effect of blending ratio and temperature on CO2 solubility in blended aqueous solution of monoethanolamine and 2-Amino-2-methyl-propanol: Experimental and modeling study using the electrolyte nonrandom two-liquid model, ACS Omega 5 (44) (2020) 28738–28748.
[49] M.E. Cardinali, C. Giomini, G. Marrosu, Successive-substitution methods in chemical-equilibrium calculations: An application to aqueous simple ampholytic electrolytes, Bulletin des Sociétés Chimiques Belges 105 (5) (1996) 227–232.
[50] M.L. Michelsen, Calculation of multiphase equilibrium, Comput. Chem. Eng. 18 (7) (1994) 545–550.
[51] NIST, N., Reference on Constants, Units and Uncertainty.
[52] Kim, S.H., et al., Online data resources in chemical engineering education: Impact of the uncertainty concept for thermophysical properties. 2019.
[53] L.i. Zong, C.-C. Chen, Thermodynamic modeling of CO2 and H2S solubilities in aqueous DIPA solution, aqueous sulfolane–DIPA solution, and aqueous sulfolane–MDEA solution with electrolyte NRTL model, Fluid Phase Equilib. 306 (2) (2011) 190–203.
[54] A. Haghtalab, H. Eghbali, A. Shojaeian, Experiment and modeling solubility of CO2 in aqueous solutions of diisopropanolamine+ 2-amino-2-methyl-1-propanol+ piperazine at high pressures, J. Chem. Thermodyn. 71 (2014) 71–83.
[55] D. Barth, C. Tondre, J.-J. Delpuech, Stopped-flow investigations of the reaction kinetics of carbon dioxide with some primary and secondary alkanolamines in aqueous solutions, Int. J. Chem. Kinet. 18 (4) (1986) 445–457.
[56] P. Blauwhoff, et al., Absorberentwurf für Anlagen zur Behandlung von sauren Erdgasen: Einfluss Prozessparameter auf Betriebsführung und Prozesswirtschaftlichkeit, Chem. Eng. Process. Process Intensif. 19 (1) (1985) 1–25.
[57] R.J. Littel, G.F. Versteeg, W.P.M. Van Swaaij, Kinetics of CO2 with primary and secondary amines in aqueous solutions—I. Zwitterion deprotonation kinetics for DEA and DIPA in aqueous blends of alkanolamines, Chem. Eng. Sci. 47 (8) (1992) 2027–2035.
[58] P.D. Vaidya, E.Y. Kenig, CO2-alkanolamine reaction kinetics: a review of recent studies, Chem. Eng. Technol. 30 (11) (2007) 1467–1474.
[59] P.N. Sutar, A. Jha, P.D. Vaidya, E.Y. Kenig, Secondary amines for CO2 capture: A kinetic investigation using N-ethylmonoethanolamine, Chem. Eng. J. 207-208 (2012) 718–724.
[60] Prausnitz, J.M., R.N. Lichtenthaler, and E.G. De Azevedo, Molecular thermodynamics of fluid-phase equilibria. 1998: Pearson Education.
[61] S.W. Brelvi, J.P. O'Connell, Correspondling states correlations for liquid compressibility and partial molal volumes of gases at infinite dilution in liquids, AIChE J. 18 (6) (1972) 1239–1243.
[62] Y. Zhang, C.-C. Chen, Thermodynamic modeling for CO2 absorption in aqueous MDEA solution with electrolyte NRTL model, Ind. Eng. Chem. Res. 50 (1) (2011) 163–175.
[63] Fowler, R.H. and E.A. Guggenheim, Statistical thermodynamics. 1949: Cambridge University Press.
[64] E.A. Macedo, P. Skovborg, P. Rasmussen, Calculation of phase equilibria for solutions of strong electrolytes in solvent—water mixtures, Chem. Eng. Sci. 45 (4) (1990) 875–882.
[65] J.-I. Baek, J.-H. Yoon, Solubility of carbon dioxide in aqueous solutions of 2-amino-2-methyl-1, 3-propanediol, J. Chem. Eng. Data 43 (4) (1998) 635–637.
[66] K.P. Shen, M.H. Li, Solubility of carbon dioxide in aqueous mixtures of monoethanolamine with methyldiethanolamine, J. Chem. Eng. Data 37 (1) (1992) 96–100.
[67] A.M. Bhairi, Experimental Equilibrium Between Acid Gases and Ethanolamine Solutions, Oklahoma State University, 1984.
[68] F.-Y. Jou, F.D. Otto, A.E. Mather, Vapor-liquid equilibrium of carbon dioxide in aqueous mixtures of monoethanolamine and methyldiethanolamine, Ind. Eng. Chem. Res. 33 (8) (1994) 2002–2005.
[69] C. Dell'Era, P. Uusi-Kyyny, J.-P. Pokki, M. Pakkanen, V. Alopaeus, Solubility of carbon dioxide in aqueous solutions of diisopropanolamine and methyldiethanolamine, Fluid Phase Equilib. 293 (1) (2010) 101–109.
[70] I.M. Bernhardsen, H.K. Knuutila, A review of potential amine solvents for CO2 absorption process: Absorption capacity, cyclic capacity and pKa, Int. J. Greenhouse Gas Control 61 (2017) 27–48.
[71] I. Kim, H.F. Svendsen, Comparative study of the heats of absorption of post-combustion CO2 absorbents, Int. J. Greenhouse Gas Control 5 (3) (2011) 390–395.
[72] M.S. Ojala, N. Ferrer Serrano, P. Uusi-Kyyny, V. Alopaeus, Comparative study: Absorption enthalpy of carbon dioxide into aqueous diisopropanolamine and monoethanolamine solutions and densities of the carbonated amine solutions, Fluid Phase Equilib. 376 (2014) 85–95.
[73] J.I. Lee, F.D. Otto, A.E. Mather, The solubility of H2S and CO2 in aqueous monoethanolamine solutions, Can. J. Chem. Eng. 52 (6) (1974) 803–805.
[74] I. Kim, H.F. Svendsen, E. Børresen, Ebulliometric determination of vapor– liquid equilibria for pure water, monoethanolamine, n-methyldiethanolamine, 3-(methylamino)-propylamine, and their binary and ternary solutions, J. Chem. Eng. Data 53 (11) (2008) 2521–2531.
[75] Katarína Klepáčová, P.J.G. Huttenhuis, P.W.J. Derks, G.F. Versteeg, Vapor pressures of several commercially used alkanolamines, J. Chem. Eng. Data 56 (5) (2011) 2242–2248.
[76] Reid R.C., Prausnitz J.M., B.E. Poling, The properties of gases and liquids, 1987.
[77] K. Schwabe, W. Graichen, D. Spiethoff, Physicochemical investigations on alkanolamines, Z. Phys. Chem. (Munich) 20 (1959) 68–82.
[78] T.J. Edwards, G. Maurer, J. Newman, J.M. Prausnitz, Vapor-liquid equilibria in multicomponent aqueous solutions of volatile weak electrolytes, AIChE J. 24 (6) (1978) 966–976.